2019

Cullin-3 Dependent Deregulation of ACTN1 Represents a New Pathogenic Mechanism in Nemaline Myopathy

Jordan Blondelle
University of California, San Diego

Kavya Tallapaka
University of California, San Diego

Jane T. Seto
University of Melbourne

Majid Ghassemian
University of California, San Diego

Madison Clark
University of California, San Diego

JCI insight

Cullin-3 dependent deregulation of ACTN1 represents a new pathogenic mechanism in nemaline myopathy

Jordan Blondelle, … , Jeffrey D. Singer, Stephan Lange

JCI Insight. 2019. https://doi.org/10.1172/jci.insight.125665.

Research In-Press Preview Muscle biology

Nemaline myopathy is a congenital neuromuscular disorder characterized by muscle weakness, fiber atrophy and presence of nemaline bodies within myofibers. However, the understanding of underlying pathomechanisms is lacking. Recently, mutations in *KBTBD13*, *KLHL40* and *KLHL41*, three substrate adaptors for the E3-ubiquitin ligase Cullin-3, have been associated with early-onset nemaline myopathies. We hypothesized that deregulation of Cullin-3 and its muscle protein substrates may be responsible for the disease development. Using *Cullin-3* knockout mice, we identified accumulation of non-muscle alpha-Actinins (ACTN1 and ACTN4) in muscles of these mice, which we also observed in *KBTBD13* patients. Our data reveal that proper regulation of Cullin-3 activity and ACTN1 levels is essential for normal muscle and neuromuscular junction development. While ACTN1 is naturally downregulated during myogenesis, its overexpression in C2C12 myoblasts triggered defects in fusion, myogenesis and acetylcholine receptor clustering; features that we characterized in Cullin-3 deficient mice. Taken together, our data highlight the importance for Cullin-3 mediated degradation of ACTN1 for muscle development, and indicate a new pathomechanism for the etiology of myopathies seen in Cullin-3 knockout mice and nemaline myopathy patients.

Cullin-3 dependent deregulation of ACTN1 represents a new pathogenic mechanism in Nemaline Myopathy

Jordan Blondelle[1*], Kavya Tallapaka[1], Jane T. Seto[2,3], Majid Ghassemian[4], Madison Clark[1], Jenni M. Laitila[5], Adam Bournazos[6,7], Jeffrey D. Singer[8], Stephan Lange[1,9*]

[1]University of California, San Diego, School of Medicine, Division of Cardiology, La Jolla, California, USA

[2]Neuromuscular Research, Murdoch Children's Research Institute, Royal Children's Hospital, Parkville VIC 3052, Australia

[3]University of Melbourne, Department of Paediatrics, Parkville, VIC 3052, Australia

[4]University of California, San Diego, Department of Chemistry and Biochemistry, La Jolla, California, USA

[5]The Folkhälsan Research Center, Helsinki, Finland and Medicum, University of Helsinki, Helsinki, Finland

[6]Kids Neuroscience Centre, Kids Research, Children's Hospital at Westmead, Sydney, New South Wales, Australia

[7]Discipline of Child and Adolescent Health, Faculty of Medicine and Health, The University of Sydney, Sydney, New South Wales, Australia

[8]Portland State University, Department of Biology, Portland, Oregon, USA

[9]University of Gothenburg, Wallenberg Laboratory, Department of Molecular and Clinical Medicine, Institute of Medicine, Gothenburg, Sweden

*Corresponding authors:

Stephan Lange, University of California, San Diego, School of Medicine, Division of Cardiology, 9500 Gilman Drive, La Jolla, CA-92093-0613C, USA

Tel: +1 (858) 822-4618, E-mail: slange@ucsd.edu

Jordan Blondelle, University of California, San Diego, School of Medicine, Division of Cardiology, 9500 Gilman Drive, La Jolla, CA-92093-0613C, USA

Tel: +1 (858) 822-4618, E-mail: jblondelle@ucsd.edu

ABSTRACT

Nemaline myopathy is a congenital neuromuscular disorder characterized by muscle weakness, fiber atrophy and presence of nemaline bodies within myofibers. However, the understanding of underlying pathomechanisms is lacking. Recently, mutations in *KBTBD13*, *KLHL40* and *KLHL41*, three substrate adaptors for the E3-ubiquitin ligase Cullin-3, have been associated with early-onset nemaline myopathies. We hypothesized that deregulation of Cullin-3 and its muscle protein substrates may be responsible for the disease development.

Using *Cullin-3* knockout mice, we identified accumulation of non-muscle alpha-Actinins (ACTN1 and ACTN4) in muscles of these mice, which we also observed in *KBTBD13* patients. Our data reveal that proper regulation of Cullin-3 activity and ACTN1 levels is essential for normal muscle and neuromuscular junction development. While ACTN1 is naturally downregulated during myogenesis, its overexpression in C2C12 myoblasts triggered defects in fusion, myogenesis and acetylcholine receptor clustering; features that we characterized in Cullin-3 deficient mice.

Taken together, our data highlight the importance for Cullin-3 mediated degradation of ACTN1 for muscle development, and indicate a new pathomechanism for the etiology of myopathies seen in Cullin-3 knockout mice and nemaline myopathy patients.

INTRODUCTION

Skeletal muscle mass represents up to 40% of the total body weight. Its maintenance is regulated by the equilibrium between muscle growth or physiological hypertrophy, and muscle atrophy, reflecting the balance between protein synthesis and degradation at the cellular level. This balance is affected in pathologies such as cancer, HIV or diabetes leading to muscle atrophy and reduced lifespan (1). Accumulation of undegraded proteins in aggrosomes or inclusion bodies is often associated with development of skeletal muscle myopathies, like nemaline or reducing-body myopathy (2). Indeed, there is mounting evidence that the deregulation of protein turnover is the primary pathogenic mechanism for some forms of skeletal myopathies. Hence, a deeper understanding of the mechanisms that govern muscle protein degradation may contribute to the development of treatments and prevention of these pathologies.

Muscle cells contain two major systems for protein degradation: the autophagy-lysosome, and the ubiquitin-proteasome systems (UPS). The latter is responsible for the degradation of 80% of muscle proteins. The UPS requires the tagging of substrates by poly-ubiquitin chains via an enzymatic cascade (3). First, the E1-activating enzyme covalently attaches to ubiquitin through an ATP-driven step. Once activated, ubiquitin is transferred to E2-conjugating enzymes. The last step requires the concerted action of E2-enzymes and E3-ligases, which transfer ubiquitin from the E2-enzyme onto the substrate (3). Once poly-ubiquitylated, the substrate is recognized by the proteasome for degradation.

Cullin-RING ligases (CRL) represent the largest E3-ubiquitin ligase family in mammals (4,

5). Cullin (1-3, 4a, 4b, 5, 7, 9) proteins are nearly ubiquitously expressed (6) and constitute the backbone of this complex. In order to form the functioning CRL complex, each Cullin binds to one of two RING (Really Interesting New Gene) domain proteins (Rbx1 or Rbx2) that associates with E2 conjugating enzymes. In addition, Cullins interact with specific substrate adaptor protein families, thereby achieving specificity for a range of cellular substrates (7). The activity of CRLs is regulated through posttranslational modification of the Cullin backbone by the small ubiquitin-like modifier Nedd8, also called neddylation (7). Cullin neddylation is removed by the COP9 signalosome complex, leading to the inactivation of the CRL (8).

For the last decades, Cullin proteins were mainly studied in the context of cancer development due to their roles in the regulation of cell proliferation through the degradation of Cyclin proteins (9). However, data regarding their roles in other tissues or pathologies remain poorly characterized. Few muscle-specific substrate adaptors that interact specifically with Cullin-1, like Atrogin-1, have been intensively investigated, and were found to exhibit key roles during muscle atrophy (10). We have recently shown that neddylation and CRL activity is necessary for normal myoblast differentiation, fusion and maturation *in vitro* (11).

Cullin-3 is highly enriched in muscle tissues (6), localizes to myofilaments and is involved in muscle protein breakdown in adult animals (12). Cullin-3 utilizes the large family of BTB-domain-containing proteins as substrate adaptors. A prominent subset of the BTB-protein family with roles in skeletal muscles is the BTB/Kelch-adaptor protein family, characterized by their combination of BTB- and Kelch-repeat domains (13). Proteins of

this family are involved in a plethora of molecular and cellular mechanisms such as cell migration, morphology or protein expression (13). Very recently, mutations in several BTB/Kelch genes (i.e. *KLHL9*, *KLHL40*, *KLHL41* and *KBTBD13*) were associated with the development of distal and nemaline myopathies in patients (13-17). The early onset of these myopathies suggests important roles for Cullin-3 and its associated protein turnover for skeletal muscle development.

While many BTB/Kelch-domain proteins may be Cullin-3 substrate adaptors, their substrates in skeletal muscles remain largely unknown. However, KLHL40 was recently shown to be necessary for postnatal muscle growth through the degradation of dimerization partner 1 (DP1) and the subsequent repression of E2F1-DP1 complex activity (18). Unexpectedly, KLHL40 also acts as a stabilizer of the thin filament proteins Leiomodin-3 and Nebulin (19). This last discovery suggests non-canonical functions for the Cullin-3 E3-ligase complex that could also be important for the stabilization of some substrate proteins rather than their degradation. These findings add a new degree of complexity to the protein turnover mechanism related to Cullin-3. Therefore, the discovery of new substrates for Cullin-3 during muscle development will be of great interest for a better understanding of myogenesis and pathogenesis of associated myopathies. While their functions are mainly unknown in muscles, expression patterns of other BTB/Kelch-domain proteins suggest important roles during muscle development (13). These findings represent an emerging role for Cullin-3 in muscle homeostasis. Indeed, characterizing the specific function(s) of Cullin-3 and its related protein turnover during muscle development would increase our understanding of

muscle biology as well as pathological mechanisms for the etiology of muscle diseases, like nemaline myopathy.

While writing this manuscript, an article investigating the role of Cullin-3 in striated muscles was published (20). The authors demonstrated that Cullin-3 was required for striated muscle development, a finding that our studies fully support. However, no molecular mechanism that explained some of the observed muscle defects were given.

We performed in-depth characterization of mice lacking Cullin-3 in skeletal muscles. Specifically, we focused on the role of Cullin-3 for the diaphragm, a hot-spot for Cullin-3 substrate adaptor function. Our data show the importance of Cullin-3 for myoblast fusion, differentiation and neuromuscular junction (NMJ) establishment through the modulation of actin dynamics and the regulation of protein levels for non-muscle alpha-actinin isoforms ACTN1 and ACTN4. Finally, we also found specific accumulation of ACTN1 and ACTN4 only in the muscles of patients suffering from *Cullin-3* related nemaline myopathy, characterized by mutations in *KBTBD13*. In addition, our study revealed that ACTN1 and ACTN4 are novel constituents of nemaline bodies in these patients.

RESULTS

Generation and validation of skeletal muscle Cul3-knockout (skm-KO) mice. To explore the role of Cullin-3 during skeletal muscle development, we crossed *Cul3*$^{flox/flox}$ mice (21) with transgenic animals that express cre-recombinase under the control of the myogenin promoter and the MEF2C enhancer (22) (Supplementary Figures S1A-B). The transcript and protein levels of Cullin-3 were subsequently monitored by RT-PCR and immunoblot analyses. Efficient recombination of the *Cullin-3* gene was observed only in skeletal muscles of *Cul3*$^{flox/flox}$*;cre+* embryos, thereafter designated as *skm-KO* (Figure 1A and Supplementary Figure S1C). In diaphragms, protein levels of Cullin-3 were diminished by 70% compared to controls (Figure 1A-B). Remaining Cullin-3 was likely due to its expression in other cell-types that are present in skeletal muscles (e.g., blood vessels, neural tissues or fibroblasts). Analysis of Cullin-3 protein levels in other tissues did not reveal significant changes (Figure 1A). We did not identify changes in mRNA levels of other *Cullin* family members (Supplementary Figure S1D).

Changes to global protein neddylation was assessed by immunoblot analysis, and revealed a 45% decrease in the 80kDa band, consistent with the predicted sizes of most Nedd8-modified Cullin proteins (23, 24) (Figure 1C-D). This substantial change suggests that Cullin-3 represents a major constituent of all active Cullins detected in the developing skeletal muscles. Analysis of K48-linked poly-ubiquitylated substrates, which are normally targeted to the proteasome for degradation revealed a decrease of low molecular weight bands (Figure 1E). Because the UPS and autophagy-lysosome system are interconnected, we assessed p62 protein levels as marker for changes to cellular

autophagy. Levels of p62 in *skm-KO* were unchanged compared to controls (Figure 1E), excluding compensatory mechanisms played by the autophagy-lysosome system to overcome deficiency of the ubiquitin-proteasome pathway. Summarized, depletion of Cullin-3 in our mouse model was strictly restricted to skeletal muscles and led to a decrease in global neddylation and poly-ubiquitylation of proteins without affecting p62 expression.

Skeletal muscle expression of Cullin-3 is required for neonatal survival.

Genotype analysis of animals at weaning stage (P21) demonstrated a complete absence of *skm-KO* mice (Supplementary Figure S2A). In comparison, *skm-KO* embryos were present in expected mendelian ratios at embryonic stage E18.5 (Supplementary Figure S2A). While *skm-KO* embryos were able to form skeletal muscles, our analyses revealed a fully penetrant postnatal lethality phenotype. Indeed, all *skm-KO* embryos died within 30 minutes following C-section (Figure 2A). *Skm-KO* neonates show few and slow spontaneous movements, and turned rapidly cyanotic (Figure 2B, Supplementary Figure S2B), which was highly suggestive of respiratory defects. Analysis of their gross anatomy revealed a strong spine curvature and wrist drop (Figure 2B), both hallmarks of muscle weakness. To evaluate if *skm-KO* embryos were able to breathe, lungs were collected and placed immediately on the surface of water. In contrast to controls, lungs of *skm-KO* embryos sank, indicating that they had never been inflated (Figure 2C). Histological analyses showed that lung alveoli of *skm-KO* embryos were not expanded (Figure 2D), again indicating that *skm-KO* embryos were unable to breathe. Our data confirm

previous reports (20) that expression of Cullin-3 in skeletal muscles is absolutely required for neonatal survival, and that the cause of death in *skm-KO* mice is due to a breathing defect.

Loss of Cullin-3 leads to severe myopathy characterized by skeletal muscle maturation defects and fiber hypotrophy.

Focusing on E18.5 *skm-KO* embryos, we found a 22.3% decrease in their body weight compared to controls (*ctl*=1.35±0.02g, *skm-KO*=1.05±0.02g; p>0.0001; Figure 3A). However, tibia lengths were not significantly changed (*ctl*=1.8±0.2cm, *skm-KO*=1.7±0.2cm; n=5 for each genotype). These data indicate that the decrease in body weight is not due to global prenatal growth retardation but may be more attributed to a 65% decrease in skeletal muscle mass (Figure 3B, Supplementary Figure S3A). Loss of skeletal muscles was also observable in diaphragm and hindlimb cross-sections stained with Hematoxylin-Eosin (Figure 3C and Supplementary Figures S3B-C). Masson's trichrome did not reveal abnormal fibrosis (not shown). However, Gomori's modified trichrome staining showed presence of aggregates (Supplementary Figure S3D). This phenotype was reminiscent of observations made in nemaline myopathies associated with mutations in genes encoding for substrate adaptors of Cullin-3 (13).

Because mutations in genes encoding for Cullin-3 substrate adaptors are mainly associated with early onset myopathies (13), we hypothesized that muscle maturation in absence of Cullin-3 may be affected. We assessed several sarcomeric proteins, markers of mature muscles, and found a severe decrease in the expression of

sarcomeric Myosin Heavy Chain, Desmin and Filamin-C (Figure 3D, Supplementary Figures S4A-C). We also noticed trends towards decreased expression of sarcomeric alpha-actinin 2 (ACTN2) and increased expression of ACTN3 (Figure 3D, Supplementary Figure S4D-E) in *skm-KO* diaphragms. However, none of these changes reached significance. During development, myonuclei first locate to the center of fibers, then migrate to the periphery in more mature muscles (25). In *skm-KO*, we observed a widespread presence of centralized nuclei while they were mainly found at the periphery in controls (Figure 3E and Figure 4A). Altogether these data are suggestive of a muscle maturation defect.

In order to investigate the pathogenic mechanism, we assessed if the reduced muscle mass relied on hypotrophy (a decrease in the size of the fibers) or hypoplasia (a decrease in the number of fibers). We stained diaphragms of control and *skm-KO* embryos with Wheat Germ Agglutinin (WGA) in order to delineate individual myofibers and analyze their sizes and numbers. The mean fiber cross-sectional area (CSA) was reduced by 62% (*ctl*=95±5.06µm^2, *skm-KO* =32±1.51µm^2; $p<0.0001$, Figure 4A and Supplementary Figure S4F) and the distribution of fiber CSAs was shifted towards smaller diameters in comparison with controls (Figure 4B). However, the number of fibers constituting the diaphragm was unchanged (*ctl*=3076±230, *skm-KO*=2654±470; Supplementary Figure S4G), suggesting that fiber hypotrophy was accountable for the reduced muscle mass.

It is established that during early steps of muscle development, myoblast fusion represents a limiting step for optimal myofiber size and muscle mass (26-33). We tested

if a defect in myoblast fusion could be responsible for the muscle fiber hypotrophy observed in embryonic *skm-KO* diaphragms. We isolated myoblasts from E18.5 control and *skm-KO* muscles and validated that *skm-KO* myoblasts undergo recombination of the *Cullin-3* locus upon expression of *myogenin* during differentiation (Figure 4C).

We then assessed myoblast fusion after 3 days of differentiation and observed a defect in *skm-KO* myotube formation (Figure 4D). *skm-KO* myoblasts expressed myogenic factors such as MyHC but did not form long myotubes (Figure 4D) as confirmed by the decrease in their fusion index defined as the number of nuclei per myotube (Supplementary Figure S4H), pointing out a fusion defect.

To confirm these results, we transfected C2C12 cells with *siRNA* against *Cullin-3* and monitored their differentiation. We found a 72% decrease in Cullin-3 protein levels in cells expressing the *siRNA* compared to cells expressing scrambled *siRNA* (Figure 4E and Supplementary Figure S4I). We then assessed myoblast fusion 5 days after differentiation and observed a 20% decrease in the fusion index (Figure 4F and Supplementary Figure S4J). While muscle proteins, such as MyHC, were not significantly changed in absence of Cullin-3, they trended towards lower expression levels (Figure 4E, and Supplementary Figure S4I).

Summarized, our data indicate that lack of Cullin-3 impedes a step required for the fusion of myoblasts and maturation of muscle fibers.

Absence of Cullin-3 affects proteins involved in degradation, calcium signaling, metabolism, muscle contraction and actin modulation.

Next, we aimed at identifying molecular mechanisms underlying the muscle defects observed in *skm-KO* embryos in order to better characterize Cullin-3 functions during skeletal muscle development. While Cullin proteins, such as Cullin-1 and Cullin-3, were broadly expressed in various adult skeletal muscles, diaphragm was a hot spot for BTB-domain proteins (Cullin-3 substrate adaptors) including KBTBD5, KBTBD13, KLHL9, KCTD6 and PLZF, with the exception of KCTD9 (Figure 5A). To maximize the chances for identifying substrates of Cullin-3 and changes to proteins that may be responsible for the observed phenotype, we performed an unbiased large-scale proteome analysis using E18.5 diaphragms. Our analysis revealed that 6% of detected proteins were significantly altered in absence of Cullin-3 (Supplementary Figure S5A). Among those, 26 proteins were significantly accumulated in *skm-KO* diaphragms, while 100 were significantly down regulated (Figure 5B).

Functional analyses aided by DAVID (https://david.ncifcrf.gov) and Metascape (http://metascape.org/) revealed that deregulated proteins might be grouped into five categories: heat shock proteins and degradation pathways, muscle and calcium associated proteins, proteins associated with metabolism and mitochondria, ribonucleoproteins and DNA-associated proteins, and proteins involved in actin modulation (Figure 5B, Supplementary Figures S5B-D). Of note, KLHL41 and KLHL31, two substrate adaptors involved in muscle physiology (15, 34, 35) were strongly decreased in *skm-KO* muscles (Supplementary Figure S5D), suggesting a destabilization of these proteins in absence of Cullin-3. Altered proteins involved in muscle and calcium physiology, metabolism and mitochondria, HSP and degradation pathways were mainly

down-regulated, whilst ribonucleoproteins and DNA-associated proteins were accumulated. To validate our proteome analysis, we studied the expression of mitochondrial subunits by immunoblot analysis using the OxPhos antibody cocktail. A strong decrease in almost all mitochondrial complex subunits was confirmed in *skm-KO* diaphragms (Supplementary Figure S5C), validating our proteome analysis.

Cullin-3 knockout muscle cells accumulate non-muscle isoforms of alpha-Actinin.

A surprising result was the strong deregulation of proteins involved in actin cytoskeleton modulation. Actin binding proteins were found both, accumulated and downregulated in *skm-KO* diaphragms (Figure 5B-C). Because of the pivotal role that remodeling of the actin cytoskeleton plays for muscle development, including myoblast fusion (36, 37), we decided to focus on these proteins.

Among them, non-muscle ACTN1 and ACTN4 isoforms were the most significantly accumulated. ACTN4s role in skeletal muscles has been investigated. Surprisingly, ACTN4 overexpression seemed to enhance myoblast differentiation (38). Hence, we focused on the role that ACTN1 may play in our phenotype.

We first confirmed the accumulation of ACTN1 in knockout muscles (Figures 6A-B) using an antibody that has been validated on muscle cells transfected with *siRNA* against *ACTN1* (Supplementary Figure S6A). In *skm-KO* myoblasts, we also observed accumulation of ACTN1 during differentiation (Figure 6C-D), suggesting that accumulation of ACTN1 in the skeletal muscles of Cullin-3 knockouts originated from muscle cells, and not from other non-muscle tissues. Intriguingly, we observed a similar

result in muscles of HSA-cre inducible Cullin-3 knockout (iCul3-KO) mice. Loss of Cullin-3 in adult muscles 1 month after excision of the gene by doxycycline treatment resulted in the accumulation of ACTN1, while sarcomeric ACTN2 remained unchanged (Figure 6E-F). Altogether, our data indicate that Cullin-3 ablation in muscle cells is responsible for the accumulation of ACTN1.

We then investigated the role that ACTN1 may play during early muscle differentiation. First, we monitored the expression of ACTN1 at the RNA and protein levels during C2C12 differentiation. While sarcomeric ACTN2 increased during differentiation, we found that ACTN1 and ACTN4 were down regulated (Supplementary Figures S6B-C). However, RNA levels of *Actn1* remained unchanged during differentiation (Supplementary Figure S6D). This result suggested an active regulation of ACTN1 protein levels and a role for Cullin-3 during muscle cell differentiation. In proliferative C2C12 cells, ACTN1 localized at the edge of the cells and along the actin stress fibers and focal contacts, confirming previous data in other cell types ((39) and Supplementary Figure S6E). Three days after differentiation, when myoblast fusion occurs, ACTN1 staining became more fragmented in a subset of cells. In other cells, it retained its localization along actin stress fibers and focal adhesion contacts (Supplementary Figure S6E). Finally, five days after differentiation, while ACTN1 still localized at the edge of mono-nucleated and non-fused cells, it was weakly expressed and diffusely localized in the cytoplasm of myotubes. Altogether, these data suggest a very active and intense remodeling of ACTN1 during myogenesis and myoblast fusion.

Overexpression of ACTN1 in differentiating myoblasts leads to fusion defects.

To test our hypothesis of a causal role for the abnormal accumulation of ACTN1 and the pathological modulation of the actin cytoskeleton proteins in the phenotype of *skm-KO* embryos, we generated a C2C12 cell line that stably overexpresses HA-ACTN1. We first validated the correct expression of HA-ACTN1 in C2C12 (Figure 7A and Supplementary Figure S7A) and monitored their differentiation. Five days after differentiation, HA-ACTN1 overexpressing cells displayed a reduction in the ability to form myotubes, compared to control cells (Figure 7B), accompanied by a slight but consistent decrease of MyHC expression (Figure 7A and Supplementary Figure S7B). Our analyses indicated a 44% decrease in the fusion index of HA-ACTN1 cells compared to controls (Figure 7C) due to an over-representation of small myotubes (2-4 nuclei), and an almost complete loss of myotubes containing larger amounts of nuclei (≥54 nuclei) (Figure 7D).

Altogether our data suggest that accumulation of ACTN1 impaired the fusion of differentiating myoblasts, resulting in smaller myotubes. These findings were reminiscent of the phenotype of muscle fibers and satellite cells from *Cullin-3* knockout animals, suggesting that accumulation of ACTN1 is responsible for, at least, part of the phenotype observed in Cullin-3 depleted tissues.

Cullin-RING ligase activity is increased during Acetylcholine receptor (AchR) clustering and leads to the increase of poly-ubiquitylated proteins.

Impairment of NMJ development often results in respiratory defects due to the dysfunction of the diaphragm and intercostal muscles (40). Importantly, a striking sustained and beneficial effect of acetylcholine-esterase inhibitor treatment has been observed in a patient affected by *KLHL40*-related nemaline myopathy, another confirmed substrate adaptor for Cullin-3 (41). In addition, sarcomeric ACTN2 has been shown to interact with rapsyn (42), and active actin cytoskeleton remodeling is absolutely required for proper Acetylcholine receptor (AchR) clustering and NMJ development (43).

Cullin E3-ligase activity is required for normal AchR clustering *in vitro* (11, 44).

We first monitored Cullin-3 expression following stimulation of C2C12 myotubes with neural agrin. We observed that Cullin-3 was significantly increased upon AchR clustering (Figure 8A and Supplementary Figure S8A), suggesting a role during NMJ development. We then looked at the expression pattern of Nedd8, the marker for Cullin activity, during AchR clustering. Following 48 hours of agrin stimulation, we found a strong increase in Nedd8 levels at 80 kDa (Figure 8B and Supplementary Figure S8B), suggesting an increase in Cullin E3-ligase activity during this process. We also observed a significant increase in poly-ubiquitylated proteins (Figure 8C and Supplementary Figure S8C), indicating an increase in protein degradation during AchR clustering. In order to test if the increase of poly-ubiquitylation was due to the increase in Cullin E3-ligase activity, we treated myotubes with both, agrin and MLN4924 (a CRL inhibitor). In absence of Cullin activity, as shown by the loss of Nedd8 signal around 80kDa (Figure 8D, left panel), the global increase of poly-ubiquitylation observed in control conditions was

inhibited (Figure 8D, right panel) demonstrating a causal role for CRLs in the increase of poly-ubiquitylation during AchR clustering. Altogether, these data indicate that Cullin-3 is increased during AchR clustering *in vitro* and that increased Cullin activity is in part responsible for protein degradation during AchR clustering.

Following these results, we decided to assess NMJs *in vivo*, specifically focusing on organization and AchR clustering in *skm-KO* diaphragms. We performed immunofluorescence analyses of post- and pre-synaptic elements. Our data revealed a complete disorganization of the NMJs in muscle lacking Cullin-3 (Figure 9A). While AchR clusters were aligned along a narrow band in the center of embryonic control diaphragms, they appeared scattered in *skm-KO* diaphragms (Figure 9A). In addition, staining of Synaptophysin/Neurofilament indicated abnormal branching and arborization of the motoneuron (Figure 9A-B), likely due to the mislocalization of the AchR clusters. Quantification showed almost a 4 times increase of the motor endplate width in *skm-KO* diaphragms, without altering the percentage of innervated AchRs clusters (Figure 9C). These data suggest that the motoneuron, while hyper-arborized and branched, was able to connect with the post-synaptic element during muscle development. We also noticed that AchR clusters were smaller in diaphragms of *skm-KO* embryos compared to controls (Figure 9D) due to an overrepresentation of small clusters and the absence of large ones.

Because we showed previously that loss of Cullin-3 leads to an accumulation of ACTN1 in muscles, we assessed if ACTN1 overexpression could be responsible for the NMJ

phenotype. We differentiated C2C12 overexpressing HA-ACTN1 or HA for 5 days, followed by agrin-induced AchR clustering. Analysis of cluster-size distribution showed a shift towards accumulation of small clusters and an absence of large ones in HA-ACTN1 expressing cells (Figure 9E), which is reminiscent of the observations made in the diaphragms of *skm-KO* embryos. In addition, a 21% decrease in the average AchR cluster length was found in myotubes expressing HA-ACTN1 (Supplementary Figure S8D-E).

Altogether, these data suggest that Cullin-3 is required for normal NMJ development and that accumulation of ACTN1 affects the formation of AchR clusters.

Non-muscle alpha-Actinins are specifically accumulated in muscles of *Cullin-3* related nemaline myopathy patients

Mutations in several substrate adaptors for Cullin-3 (i.e. *KBTBD13*, *KLHL9*, *KLHL40*, *KLHL41*) are associated with the development of distal and nemaline myopathies (13-17). In order to test the relevance of our findings for human health, we analyzed muscle samples from nemaline myopathy patients with mutations in the Cullin-3 substrate adaptor *KBTBD13* (16), *TPM2* (Chr9(GRCh37):g.35685480A>G, NM_003289.3(TPM2):c.443T>C) or *NEB* (chr2:152389953T>C, c.21522+3A>G (NM_001271208.1); chr2:152581433delG, c.445delC (NM_001271208.1)). Mutations in *KBTBD13* are mainly associated with early onset nemaline myopathies, characterized by muscle weakness, slow movement, pronounced muscle fiber atrophy and the presence of nemaline bodies (16). KBTBD13 is a substrate adaptor for Cullin-3 (45). We confirmed the presence of nemaline bodies in our *KBTBD13* patients through Gomori trichrome

staining (Figure 10A). We then investigated protein levels of Actinin isoforms. While levels of ACTN2 and ACTN3 were mainly unchanged across the patients and controls, we found a striking increase in ACTN1 and ACTN4 levels only in *KBTBD13* patients (Figure 10B), mimicking results obtained in the muscles of *skm-KO* embryos. Finally, we asked if nemaline bodies, features shared by all nemaline myopathy patients are positive for non-muscle alpha-Actinin isoforms. While, nemaline bodies are known to be positive for ACTN2, we found that they were also reactive to ACTN1 and ACTN4 in muscle biopsies of *KBTBD13* patients (Figure 10C).

Altogether, these data reveal an abnormal accumulation of non-muscle ACTN1 and ACTN4 in nemaline myopathy patients with mutations in *KBTBD13*, which encodes for a Cullin-3 related protein. In addition, we unravel that ACTN1 and ACTN4 accumulate in nemaline bodies of these patients, lengthening the list of proteins constituting these structures.

DISCUSSION

It has been recently shown that mice lacking Cullin-3 develop severe muscle atrophy and cardiomyopathy but the responsible molecular mechanism has not been identified (20).

While Nedd8, the crucial regulator for CRL activity is largely downregulated in a lot of mature tissues, its expression remains high in differentiated muscles (i.e. heart and skeletal muscles) (24), suggesting important roles for CRLs in these tissues. Our data show for the first time that substrate adaptors of Cullin-3 display diverse expression patterns in various skeletal muscle types, with diaphragm muscles emerging as a hotspot for their expression. Absence of Cullin-3 impairs the UPS, and is characterized by a decrease in protein neddylation and poly-ubiquitylation, in differentiating skeletal muscles. These findings suggest that Cullin-3 is a major active CRL during muscle development.

Cullin-3 *skm-KO* mice exhibit severe hypotrophy of myofibers and die within a few minutes after birth. Cullin-3 depleted myoblasts (*skm-KO* satellite cells and C2C12 treated with *Cullin-3 siRNA*), while able to express myogenic factors, were unable to form large myotubes, suggestive of impaired myoblast fusion. Comparisons with mouse models exhibiting a similar phenotype indicate that muscle hypotrophy and fusion defects may be, at least, partially responsible for the death of Cullin-3 *skm-KO* mice (26-33).

Intriguingly, *skm-KO* embryos share a similar phenotype with some knockout models for NMJ components, such as *Agrin*, *Choline acetyltransferase*, *MuSK* or *Rapsyn* (40). The models are characterized by rapid postnatal lethality due to respiratory defects resulting from insufficient muscle development and improper transmission of neuronal signals to the muscle (40). Due to the striking beneficial effects of acetylcholine-esterase inhibitor treatment in a *KLHL40*-related nemaline myopathy patient (41), we asked if Cullin-3 could also be required for NMJ formation and function. Our data uncovered a new function for Cullin-3 during development of NMJs, an essential process for myogenesis and muscle growth (40). We demonstrated that Cullin-3 and CRL activity increases during AchR clustering, and is required for the increased level of poly-ubiquitylated proteins occurring during this process. Increasing evidence suggests that protein ubiquitylation may play an important role in regulating synapse development (46). Interestingly, it was demonstrated that RPY-1, the homolog of Rapsyn in *C. elegans*, can be degraded by Cullin-3 (47, 48). While those findings link Cullin-3 with NMJ development in nematodes, this mechanism has not been further investigated in mammals.

In this study, we found that loss of Cullin-3 *in vivo* an *in vitro* led to disorganized and smaller AchR clusters, resulting in hyper-arborization of the motoneuron. Of note, Cullin-5 and -2 have already been linked to the development of NMJs in *Drosophila melanogaster*, but their roles have also never been further corroborated in mammals (49). Altogether, these data may uncover a more universal function for CRLs during NMJ development.

On the molecular level, our proteome analysis of diaphragm muscles revealed the deregulation of proteins involved in muscle metabolism and mitochondria, calcium handling, protein degradation, actin cytoskeleton modulation, as well as ribonucleosome and DNA-associated proteins. Our proteome analysis diverges from the recently published Cullin-3 knockout model (20). An explanation for this discrepancy is that the authors performed proteome analysis of *whole* hindlimb muscles, while we specifically isolated and investigated the diaphragm. We chose to use diaphragm over hindlimb muscles for several reasons: 1) the diaphragm is a hot-spot for the expression of Cullin-3 substrate adaptors, increasing the chances to identify molecular mechanisms played by Cullin-3 in skeletal muscles. 2) In contrast to hindlimbs, the use and analysis of diaphragm muscles reduces contamination by other tissue types, minimizing the risks of identifying changes that are actually due to non-muscle cells, such as fibroblasts from connective tissue, adipocytes or endothelial cells.

The deregulation of non-muscle ACTN1 and ACTN4, Vinculin, Filamin-C, Cofilin-2, Myotilin or Xirp1 triggered our attention. Cullin-3 and BTB-domain containing proteins have already been shown to act as organizers of the cytoskeleton in *Drosophila melanogaster* (50, 51). The remodeling of the actin cytoskeleton is an essential step for efficient myoblast fusion (37) and for AchR clustering at the NMJ (52, 53). While Vinculin, Filamin-C, Cofilin-2 and Myotilin have been associated with myoblast fusion and differentiation (54-57) and NMJ (58, 59), little is known about the role of ACTN1 in muscles.

The family of alpha-Actinin proteins includes the muscle specific ACTN2 and ACTN3, and two non-muscle isoforms ACTN1 and ACTN4. Alpha-Actinins are essential for the stability and the architecture of the cytoskeleton, and mutations in these genes lead to pathologies in humans (60-62). ACTN1 and ACTN4 crosslink actin filaments in the cytoskeleton of non-muscle cells, while sarcomeric ACTN2 and ACTN3 anchor the thin-filaments and titin at the Z-disks of mature muscles (39). Alpha-Actinins form homo- or heterodimers and each dimer binds to common or specific ligands (63, 64), suggesting specific biological roles. In this study, we show that during *normal* myoblast differentiation ACTN2 and ACTN3 are up-regulated, while ACTN1 and ACTN4 are downregulated. In contrast to sarcomeric isoforms, the non-muscle isoforms have been poorly investigated in developing muscles (39). ACTN4 seems to enhance differentiation of C2C12 myoblasts through the regulation of myogenic genes (38). Here, we show that the loss of Cullin-3 in muscle cells results in accumulation of non-muscle ACTN1. Overexpression of ACTN1 in myoblasts was sufficient to recapitulate most of the phenotype of *skm-KO* cells, characterized by fusion and AchR clustering defects as well as myofiber hypotrophy, suggesting that ACTN1 and ACTN4 play different, even opposite roles in developing muscles. Contrasting roles for ACTN1 and ACTN4 have already been described in other tissues (65-67), as well as differential biochemical properties in muscles (68). The post-synaptic component of the phenotype of our model reveals novel roles for Cullin-3 targeted protein turnover and ACTN1 regulation during NMJ formation.

Mutations in Cullin-3 substrate adaptors genes such as *KBTBD13* have been associated with early onset nemaline myopathies. Nemaline myopathies are characterized by nemaline bodies (protein aggregates) in myofibers, and are often associated with muscle weakness (69). Proteins constituting nemaline bodies include Actin (70), Filamin-C (71), Telethonin (72), Myozenin (73), Myopalladin (74) or Myotilin (75). While sarcomeric ACTN2 is also thought to be a major constituent (71, 76, 77), studies investigating whether levels of muscle alpha-Actinins are changed in these patients show conflicting results, depending on the used method, and whether the employed antibodies have been specific to one alpha-Actinin isoform (76-79). Non-muscle ACTN1 and ACTN4 have never been investigated *per se* in nemaline myopathy patients but abnormal deposition of ACTN1 proteins in clusters has been observed in cardiomyocytes from patients with dilated cardiomyopathy or chronic pressure overload (80), representing a biomarker for the disease. While these data do not demonstrate that ACTN1 accumulation is causative for the cardiac disease, they are suggestive of an involvement in the pathogenic mechanism. In addition, ACTN1 interacts with UDP-N-acetylglucosamine 2-epimerase/N-acetylmannosamine kinase (GNE), an enzyme linked to hereditary inclusion body myopathy (HIBM)(81).

Our data show that ACTN1 and ACTN4 were accumulated in muscle tissues and nemaline bodies of patients with mutations in *KBTBD13* but not in *TPM2* and *Nebulin*. Those results suggest that accumulation of ACTN1 and ACTN4 may represent a specific pathogenic mechanism due to Cullin-3 impairment.

While further studies are required to know the extent of non-muscle alpha-Actinin expression in nemaline myopathy patients, ACTN1 and ACTN4 should now be considered as constituents of nemaline bodies in some patients.

Indeed, a correlation between ACTN1 or ACTN4 protein levels and severity of the disease would be of clinical interest. An interesting feature of patients with *KBTBD13* mutation resides in the lack of cardiac phenotype (16). In contrast to skeletal muscles, heart development does not rely on cell fusion events. This developmental difference may contribute to protecting the heart from the consequences of ACTN1 accumulation.

To summarize, we propose that Cullin-3 critically contributes to actin cytoskeleton remodeling to allow for optimal myoblast fusion, differentiation and clustering of AchRs. We propose that non-muscle ACTN1 and ACTN4 are a new target for Cullin-3 during myogenesis. Mutations in Cullin-3 substrate adaptors such as *KBTBD13*, leads to pathological non-muscle Actinin accumulation in patients (Figure 11). This finding may represent a new unifying pathogenic mechanism for the etiology of Cullin-3 related myopathies. Further investigations regarding a potential accumulation of non-muscle alpha-Actinins in nemaline patients with mutations in other Cullin-3 substrate adaptors (e.g. *KLHL9, KLHL40* and *KLHL41*) will be required to confirm this hypothesis.

METHODS

Generation of *skm-Cul3* and iCul3-KO mice

The strategy used to generate the floxed-*Cul3* mice has been described and published (21). We generated constitutive skeletal muscle specific (*skmKO-Cul3*) and inducible skeletal muscle specific (iCul3-KO) Cullin-3 knockouts, by breeding floxed-*Cul3* mice with mice expressing the Cre-recombinase under control of the Myogenin promoter (22), or a tetracycline/doxycycline inducible human skeletal actin (HSA) promoter (82), respectively. All procedures involving genetically modified animals have been approved by the UC San Diego Institutional Animal Care and Use Committee (IACUC).

Extraction of total RNA, RT-PCR and qRT-PCR analysis

Mouse muscle samples were snap frozen in liquid nitrogen and stored at -80°C. Cells were washed with PBS, then lysed using TRIzol reagent (ThermoFisher Scientific). Total RNA from muscles or cells was extracted according to the manufacturers instructions. Purity of RNA was assessed by a ratio of absorbance at 260nm and 230nm >1.7. 200ng of RNA was used for reverse transcriptase reaction using the Maxima First Strand cDNA synthesis kit (Fermentas; ThermoFisher Scientific) and random hexamers. Oligonucleotides for RT-PCR and RT-qPCR are listed in Supplementary Table 1.

Oligonucleotides optimized for qPCR of murine Actinin1 and cyclophilin B were used in reactions employing the PerfeCTa SYBR green real-time qPCR mix (Quanta BioSciences; Beverly, MA) and a CFX96 thermocycler (BioRad; Hercules, CA). Samples were

normalized to cyclophilin B. If not noted otherwise, three biological samples were analyzed per sample group.

C2C12 and primary myoblast cell culture

C2C12 cells were grown, differentiated and their fusion index was assessed as described previously (26).

Mouse primary myoblasts were obtained by dissecting the diaphragm and tongue muscles from E18.5 embryos. Myoblasts were isolated and cultured as previously described (11).

siRNA

Proliferating C2C12 cells were transfected with siRNA directed against Cullin-3 (ON-TARGETplus mouse Cullin-3 (26554); GE Healthcare Dharmacon), ACTN1 (ON-TARGETplus mouse Actn1 (L-066191-00-0005) or scrambled control (ON-TARGETplus non-targeting siRNA #1; GE Healthcare Dharmacon) using DharmaFECT 1 transfection reagent (GE Healthcare Dharmacon) according to the manufacturers instructions. 24 hours after transfection, cells were changed into differentiation medium, and allowed to differentiate for 5 days before analysis. Efficiency of siRNA was verified by immunoblot analysis.

Immunoblot analysis

Proteins were extracted from tissues and cells then quantified as previously described

(11). 5 to 10µg of clarified lysates were separated by SDS-PAGE. Transfer was performed on nitrocellulose membranes (BioRad). Membranes were incubated with blocking solution (TBS-Tween containing 5% BSA) for 1 hour at room temperature, then incubated with primary antibodies (Supplementary Table 2) in blocking solution overnight at 4°C. After washing, secondary HRP-linked antibodies (DAKO, Cell Signaling) were applied for 1 hour at room temperature. After washing, antibody-bound proteins were visualized on X-ray films or by BioRAD imager. Quantification of band intensities was performed using ImageJ software (1.48v) or BioRAD Image Lab (v5.2.1). Uncut immunoblot images can be found in the supplementary data section.

Quantitative proteome analysis of skeletal muscle

Proteins were isolated form diaphragms by lysis into ice-cold isolation buffer (300mM KCl, 30mM PIPES pH6.6, 0.5% NP-40, 1x protease inhibitor (Roche), 1x Phos-Stop (Roche)). Insoluble proteins were removed by centrifugation (14,000 rpm, 10 minutes at 4ºC), and the supernatant was diluted 1:4 with ice cold dilution buffer (1x Phos-Stop (Roche), 0.5% NP-40, 1mM DTT). Precipitation of acto-myosin components was done by centrifugation (14,000rpm, 15 minutes at 4ºC), and the remaining supernatant snap-frozen for further analysis by mass-spectrometry.

Proteins destined for mass-spectrometry were digested by tryptic digest, differentially labeled for iTRAQ and analyzed in a SciEx QTOF5600 system. Collected spectrograms were further analyzed and quantified using Peaks (83). A full dataset of identified proteins was deposited at the Mendeley repository (84). Bioinformatic enrichment and

pathway analysis was done using Metascape (http://metascape.org/; (85)), Morpheus (https://software.broadinstitute.org/morpheus/), the BioGRID (https://thebiogrid.org/; (86)) and Venny (http://bioinfogp.cnb.csic.es/tools/venny).

Statistical analysis

With the exception for built in statistics by Peaks Studio software, statistical analysis of all data was done by either using ANOVA comparison followed by correction for multiplicity of testing using Bonferroni's multiple comparisons test, or unpaired t-test, performed using Excel (Microsoft) or GraphPad Prism version 7 for Mac (GraphPad Software, http://www.graphpad.com/). Results are presented as means ± standard error. P-values of $p<0.05$ were considered statistically significant. Sample sizes are indicated in the figure or figure legend. If not state otherwise, both sexes were analyzed in the experimental procedures.

Generation of HA-ACTN1 stable cell line

For expression of HA-ACTN1 in C2C12 cells, cDNA was isolated by RT-PCR on mRNA extracted from proliferative C2C12. Oligonucleotides used for amplification were the following: ACTN1.fwd: GATGGCTAGCATGGACCATTATGATTCCCAG; ACTN1.rev: CATGAGCTCGAGGTCGCTCTCGCCATACAG. PCR products were cloned into a custom built HA-vector (12). HA-ACTN1 or HA-control transfected cells were selected with G-418 (Invitrogen). Plasmid expression was checked by RT-qPCR, immunoblot and immunostaining.

Immunofluorescence microscopy

Cells were rinsed one time with PBS, fixed for 15 minutes with 4% paraformaldehyde and rinsed 3 times with PBS. Mouse muscles were snap-frozen in isopentane cooled in liquid nitrogen and stored at −80 °C until sectioning. Muscles were sectioned using a Leica cryostat. Sections were fixed in ice-cold acetone for 5 minutes, followed by rehydration in 1x PBS for 10 minutes. Cells or muscle slides were then permeabilized for 10 minutes in 1xPBS supplemented with 0.2% Triton X-100 (Sigma Aldrich; St. Louis, MO), washed 3 times with PBS and incubated in blocking solution (Gold Buffer [GB, 150mM NaCl, 20mM Tris pH7.4] supplemented with 1% BSA) for 1 hour at room temperature before incubation with primary antibodies (Supplementary Table 2) in blocking solution. Primary antibodies were either incubated for 2 hours at room temperature, or overnight at 4°C. Following incubation, cells were washed three times for 5 minutes with PBS, and incubated with secondary antibodies (all from Jackson ImmunoResearch Laboratories Inc.; West Grove, PA) diluted into blocking solution for 1 hour at room temperature. Secondary antibody mixtures also contained DAPI (4', 6' diamidino-2-phenylindol) and/or fluorescently linked alpha-bungarotoxin (BGTX; Molecular Probes, ThermoFisher Scientific), Alexa Fluor 555 conjugate of wheat germ agglutinin (WGA; ThermoFisher Scientific) or fluorescently labeled phalloidin (Molecular Probes; ThermoFisher Scientific) when appropriate. After washing three times with PBS for 5 minutes, cells were mounted using fluorescent mounting medium (Dako; Carpinteria, CA). Microscopy was performed using an Olympus FV1000 confocal

microscope using either the 20x air objective, the 40x or 63x oil immersion objective, zoom rates between 1 and 3, and imaged in sequential scanning mode. Images were analyzed using ImageJ (NIH).

Stimulation of AchR clustering and quantification in C2C12 myotubes

Stimulation and quantification of AchR clustering by rat agrin (R&D Systems) was performed as described previously (11).

Histology analyses

Transverse-sections (10 µm thickness) were stained with hematoxylin-eosin (H&E; Sigma Aldrich) or Gomori's modified Trichrome (VWR). Diameter and distribution of myofibers were determined. Quantification of fiber numbers, sizes or nuclear localization was performed on 3 sections separated by at least 30 µm. Morphometric quantification and evaluation of fiber sizes and numbers was done using ImageJ (1.48v).

Human ethics approval

Samples from patients and controls were obtained after receiving informed consent for diagnostic and research investigation. Studies were performed in accordance with the Declaration of Helsinki and approved by the respective human research institutional review board responsible for each research site.

AUTHORS CONTRIBUTIONS

J.B. and S.L. designed research studies. J.B., K.T., J.T.S., M.G., J.L. and M.C. conducted the experiments and analyzed the data. A.B. provided human samples. J.D.S. provided animals and reagents. J.B. and S.L. wrote the manuscript.

ACKNOWLEDGMENTS

J.B. is supported by the Muscular Dystrophy Association grant (MDA 515518) and Philippe Foundation grant. Work in the laboratory of S.L. is supported by an NIH R01 grant (HL128457). M.C. was supported by the American Heart Association (17UFEL33520004). The work at the mass-spectrometry core is supported by NIH grants (S10 OD016234, S10 OD021724). We thank the UC San Diego Microscopy Core and Jennifer Santini, who are supported by an NIH-NINDS P30 grant (NS047101). J.L. was supported by grants from the Association Francaise contre les Myopathies, the Finska Läkaresällskapet, the Medicinska understödsföreningen Liv och Hälsa r.f. and the Magnus Ehrnrooth foundation. We thank Dr. Valeria Marroco, Prof. Farah Sheik, Dr. Yan Liang, Dr. Jing Zhang, Dr. Maria Manso, Dr. Paul Bushway and William Bradford, as well as Prof. Wallgren-Pettersson and Prof. Pelin for insightful discussions. We also thank Professor Sandra Cooper and Professor Kathryn N. North for providing patient samples and controls for this study, as well as Prof. Beggs for generously providing antibodies.

REFERENCES

1. Muscaritoli M, Lucia S, Molfino A, Cederholm T, and Rossi Fanelli F. Muscle atrophy in aging and chronic diseases: is it sarcopenia or cachexia? Internal and emergency medicine. 2013;8(7):553-60.
2. North K. What's new in congenital myopathies? Neuromuscular disorders : NMD. 2008;18(6):433-42.
3. Bonaldo P, and Sandri M. Cellular and molecular mechanisms of muscle atrophy. Disease models & mechanisms. 2013;6(1):25-39.
4. Petroski MD, and Deshaies RJ. Function and regulation of cullin-RING ubiquitin ligases. Nature reviews Molecular cell biology. 2005;6(1):9-20.
5. Bosu DR, and Kipreos ET. Cullin-RING ubiquitin ligases: global regulation and activation cycles. Cell division. 2008;3(7.
6. Hori T, Osaka F, Chiba T, Miyamoto C, Okabayashi K, Shimbara N, Kato S, and Tanaka K. Covalent modification of all members of human cullin family proteins by NEDD8. Oncogene. 1999;18(48):6829-34.
7. Zhou W, Wei W, and Sun Y. Genetically engineered mouse models for functional studies of SKP1-CUL1-F-box-protein (SCF) E3 ubiquitin ligases. Cell research. 2013;23(5):599-619.
8. Kato JY, and Yoneda-Kato N. Mammalian COP9 signalosome. Genes to cells : devoted to molecular & cellular mechanisms. 2009;14(11):1209-25.
9. Chen Z, Sui J, Zhang F, and Zhang C. Cullin family proteins and tumorigenesis: genetic association and molecular mechanisms. Journal of Cancer. 2015;6(3):233-42.
10. Bodine SC, Latres E, Baumhueter S, Lai VK, Nunez L, Clarke BA, Poueymirou WT, Panaro FJ, Na E, Dharmarajan K, et al. Identification of ubiquitin ligases required for skeletal muscle atrophy. Science. 2001;294(5547):1704-8.
11. Blondelle J, Shapiro P, Domenighetti AA, and Lange S. Cullin E3 Ligase Activity Is Required for Myoblast Differentiation. Journal of molecular biology. 2017;429(7):1045-66.
12. Lange S, Perera S, Teh P, and Chen J. Obscurin and KCTD6 regulate cullin-dependent small ankyrin-1 (sAnk1.5) protein turnover. Molecular biology of the cell. 2012;23(13):2490-504.
13. Gupta VA, and Beggs AH. Kelch proteins: emerging roles in skeletal muscle development and diseases. Skeletal muscle. 2014;4(11.
14. Ravenscroft G, Miyatake S, Lehtokari VL, Todd EJ, Vornanen P, Yau KS, Hayashi YK, Miyake N, Tsurusaki Y, Doi H, et al. Mutations in KLHL40 are a frequent cause of severe autosomal-recessive nemaline myopathy. American journal of human genetics. 2013;93(1):6-18.
15. Gupta VA, Ravenscroft G, Shaheen R, Todd EJ, Swanson LC, Shiina M, Ogata K, Hsu C, Clarke NF, Darras BT, et al. Identification of KLHL41 Mutations Implicates BTB-Kelch-Mediated Ubiquitination as an Alternate Pathway to Myofibrillar Disruption in Nemaline Myopathy. American journal of human genetics. 2013;93(6):1108-17.
16. Sambuughin N, Yau KS, Olive M, Duff RM, Bayarsaikhan M, Lu S, Gonzalez-Mera L, Sivadorai P, Nowak KJ, Ravenscroft G, et al. Dominant mutations in KBTBD13, a member of the BTB/Kelch family, cause nemaline myopathy with cores. American journal of human genetics. 2010;87(6):842-7.
17. Marttila M, Hanif M, Lemola E, Nowak KJ, Laitila J, Gronholm M, Wallgren-Pettersson C, and Pelin K. Nebulin interactions with actin and tropomyosin are altered by disease-causing mutations. Skeletal muscle. 2014;4(15.
18. Gong W, Gohla RM, Bowlin KM, Koyano-Nakagawa N, Garry DJ, and Shi X. Kelch Repeat and BTB Domain Containing Protein 5 (Kbtbd5) Regulates Skeletal Muscle Myogenesis through the E2F1-DP1 Complex. The Journal of biological chemistry. 2015;290(24):15350-61.

19. Garg A, O'Rourke J, Long C, Doering J, Ravenscroft G, Bezprozvannaya S, Nelson BR, Beetz N, Li L, Chen S, et al. KLHL40 deficiency destabilizes thin filament proteins and promotes nemaline myopathy. The Journal of clinical investigation. 2014;124(8):3529-39.
20. Papizan JB, Vidal AH, Bezprozvannaya S, Bassel-Duby R, and Olson EN. Cullin-3-RING ubiquitin ligase activity is required for striated muscle function in mice. The Journal of biological chemistry. 2018;293(23):8802-11.
21. Singer JD, Gurian-West M, Clurman B, and Roberts JM. Cullin-3 targets cyclin E for ubiquitination and controls S phase in mammalian cells. Genes & development. 1999;13(18):2375-87.
22. Li S, Czubryt MP, McAnally J, Bassel-Duby R, Richardson JA, Wiebel FF, Nordheim A, and Olson EN. Requirement for serum response factor for skeletal muscle growth and maturation revealed by tissue-specific gene deletion in mice. Proceedings of the National Academy of Sciences of the United States of America. 2005;102(4):1082-7.
23. Liakopoulos D, Doenges G, Matuschewski K, and Jentsch S. A novel protein modification pathway related to the ubiquitin system. The EMBO journal. 1998;17(8):2208-14.
24. Kamitani T, Kito K, Nguyen HP, and Yeh ET. Characterization of NEDD8, a developmentally down-regulated ubiquitin-like protein. The Journal of biological chemistry. 1997;272(45):28557-62.
25. Roman W, and Gomes ER. Nuclear positioning in skeletal muscle. Seminars in cell & developmental biology. 2018;82(51-6.
26. Blondelle J, Ohno Y, Gache V, Guyot S, Storck S, Blanchard-Gutton N, Barthelemy I, Walmsley G, Rahier A, Gadin S, et al. HACD1, a regulator of membrane composition and fluidity, promotes myoblast fusion and skeletal muscle growth. Journal of molecular cell biology. 2015;7(5):429-40.
27. Horsley V, Friday BB, Matteson S, Kegley KM, Gephart J, and Pavlath GK. Regulation of the growth of multinucleated muscle cells by an NFATC2-dependent pathway. The Journal of cell biology. 2001;153(2):329-38.
28. Doherty KR, Cave A, Davis DB, Delmonte AJ, Posey A, Earley JU, Hadhazy M, and McNally EM. Normal myoblast fusion requires myoferlin. Development. 2005;132(24):5565-75.
29. Georgiadis V, Stewart HJ, Pollard HJ, Tavsanoglu Y, Prasad R, Horwood J, Deltour L, Goldring K, Poirier F, and Lawrence-Watt DJ. Lack of galectin-1 results in defects in myoblast fusion and muscle regeneration. Developmental dynamics : an official publication of the American Association of Anatomists. 2007;236(4):1014-24.
30. Laurin M, Fradet N, Blangy A, Hall A, Vuori K, and Cote JF. The atypical Rac activator Dock180 (Dock1) regulates myoblast fusion in vivo. Proceedings of the National Academy of Sciences of the United States of America. 2008;105(40):15446-51.
31. Hochreiter-Hufford AE, Lee CS, Kinchen JM, Sokolowski JD, Arandjelovic S, Call JA, Klibanov AL, Yan Z, Mandell JW, and Ravichandran KS. Phosphatidylserine receptor BAI1 and apoptotic cells as new promoters of myoblast fusion. Nature. 2013;497(7448):263-7.
32. Millay DP, O'Rourke JR, Sutherland LB, Bezprozvannaya S, Shelton JM, Bassel-Duby R, and Olson EN. Myomaker is a membrane activator of myoblast fusion and muscle formation. Nature. 2013;499(7458):301-5.
33. Lenhart KC, Becherer AL, Li J, Xiao X, McNally EM, Mack CP, and Taylor JM. GRAF1 promotes ferlin-dependent myoblast fusion. Developmental biology. 2014;393(2):298-311.
34. Ramirez-Martinez A, Cenik BK, Bezprozvannaya S, Chen B, Bassel-Duby R, Liu N, and Olson EN. KLHL41 stabilizes skeletal muscle sarcomeres by nonproteolytic ubiquitination. eLife. 2017;6(
35. Papizan JB, Garry GA, Brezprozvannaya S, McAnally JR, Bassel-Duby R, Liu N, and Olson EN. Deficiency in Kelch protein Klhl31 causes congenital myopathy in mice. The Journal of clinical investigation. 2017;127(10):3730-40.
36. Peckham M. Engineering a multi-nucleated myotube, the role of the actin cytoskeleton. Journal of microscopy. 2008;231(3):486-93.
37. Martin SG. Role and organization of the actin cytoskeleton during cell-cell fusion. Seminars in cell & developmental biology. 2016;60(121-6.
38. An HT, Kim J, Yoo S, and Ko J. Small leucine zipper protein (sLZIP) negatively regulates skeletal muscle differentiation via interaction with alpha-actinin-4. The Journal of biological chemistry. 2014;289(8):4969-79.

39. Sjoblom B, Salmazo A, and Djinovic-Carugo K. Alpha-actinin structure and regulation. Cellular and molecular life sciences : CMLS. 2008;65(17):2688-701.
40. Tintignac LA, Brenner HR, and Ruegg MA. Mechanisms Regulating Neuromuscular Junction Development and Function and Causes of Muscle Wasting. Physiological reviews. 2015;95(3):809-52.
41. Natera-de Benito D, Nascimento A, Abicht A, Ortez C, Jou C, Muller JS, Evangelista T, Topf A, Thompson R, Jimenez-Mallebrera C, et al. KLHL40-related nemaline myopathy with a sustained, positive response to treatment with acetylcholinesterase inhibitors. Journal of neurology. 2016;263(3):517-23.
42. Dobbins GC, Luo S, Yang Z, Xiong WC, and Mei L. alpha-Actinin interacts with rapsyn in agrin-stimulated AChR clustering. Molecular brain. 2008;1(18.
43. Dai Z, Luo X, Xie H, and Peng HB. The actin-driven movement and formation of acetylcholine receptor clusters. The Journal of cell biology. 2000;150(6):1321-34.
44. Li L, Cao Y, Wu H, Ye X, Zhu Z, Xing G, Shen C, Barik A, Zhang B, Xie X, et al. Enzymatic Activity of the Scaffold Protein Rapsyn for Synapse Formation. Neuron. 2016;92(5):1007-19.
45. Sambuughin N, Swietnicki W, Techtmann S, Matrosova V, Wallace T, Goldfarb L, and Maynard E. KBTBD13 interacts with Cullin 3 to form a functional ubiquitin ligase. Biochemical and biophysical research communications. 2012;421(4):743-9.
46. DiAntonio A, and Hicke L. Ubiquitin-dependent regulation of the synapse. Annual review of neuroscience. 2004;27(223-46.
47. Feng G, Steinbach JH, and Sanes JR. Rapsyn clusters neuronal acetylcholine receptors but is inessential for formation of an interneuronal cholinergic synapse. The Journal of neuroscience : the official journal of the Society for Neuroscience. 1998;18(11):4166-76.
48. Nam S, Min K, Hwang H, Lee HO, Lee JH, Yoon J, Lee H, Park S, and Lee J. Control of rapsyn stability by the CUL-3-containing E3 ligase complex. The Journal of biological chemistry. 2009;284(12):8195-206.
49. Ayyub C. Cullin-5 and cullin-2 play a role in the development of neuromuscular junction and the female germ line of Drosophila. Journal of genetics. 2011;90(2):239-49.
50. Hudson AM, Mannix KM, and Cooley L. Actin Cytoskeletal Organization in Drosophila Germline Ring Canals Depends on Kelch Function in a Cullin-RING E3 Ligase. Genetics. 2015;201(3):1117-31.
51. Hudson AM, and Cooley L. Drosophila Kelch functions with Cullin-3 to organize the ring canal actin cytoskeleton. The Journal of cell biology. 2010;188(1):29-37.
52. Cartaud A, Stetzkowski-Marden F, Maoui A, and Cartaud J. Agrin triggers the clustering of raft-associated acetylcholine receptors through actin cytoskeleton reorganization. Biology of the cell. 2011;103(6):287-301.
53. Madhavan R, and Peng HB. A synaptic balancing act: local and global signaling in the clustering of ACh receptors at vertebrate neuromuscular junctions. Journal of neurocytology. 2003;32(5-8):685-96.
54. Vasyutina E, Martarelli B, Brakebusch C, Wende H, and Birchmeier C. The small G-proteins Rac1 and Cdc42 are essential for myoblast fusion in the mouse. Proceedings of the National Academy of Sciences of the United States of America. 2009;106(22):8935-40.
55. Dalkilic I, Schienda J, Thompson TG, and Kunkel LM. Loss of FilaminC (FLNc) results in severe defects in myogenesis and myotube structure. Molecular and cellular biology. 2006;26(17):6522-34.
56. Zhu H, Yang H, Zhao S, Zhang J, Liu D, Tian Y, Shen Z, and Su Y. Role of the cofilin 2 gene in regulating the myosin heavy chain genes in mouse myoblast C2C12 cells. International journal of molecular medicine. 2018;41(2):1096-102.
57. Keduka E, Hayashi YK, Shalaby S, Mitsuhashi H, Noguchi S, Nonaka I, and Nishino I. In vivo characterization of mutant myotilins. The American journal of pathology. 2012;180(4):1570-80.
58. Bloch RJ, and Hall ZW. Cytoskeletal components of the vertebrate neuromuscular junction: vinculin, alpha-actinin, and filamin. The Journal of cell biology. 1983;97(1):217-23.

59. Yorifuji H, and Hirokawa N. Cytoskeletal architecture of neuromuscular junction: localization of vinculin. Journal of electron microscopy technique. 1989;12(2):160-71.
60. Yasutomi M, Kunishima S, Okazaki S, Tanizawa A, Tsuchida S, and Ohshima Y. ACTN1 rod domain mutation associated with congenital macrothrombocytopenia. Annals of hematology. 2016;95(1):141-4.
61. Yao J, Le TC, Kos CH, Henderson JM, Allen PG, Denker BM, and Pollak MR. Alpha-actinin-4-mediated FSGS: an inherited kidney disease caused by an aggregated and rapidly degraded cytoskeletal protein. PLoS biology. 2004;2(6):e167.
62. Haywood NJ, Wolny M, Rogers B, Trinh CH, Shuping Y, Edwards TA, and Peckham M. Hypertrophic cardiomyopathy mutations in the calponin-homology domain of ACTN2 affect actin binding and cardiomyocyte Z-disc incorporation. The Biochemical journal. 2016;473(16):2485-93.
63. Ribeiro Ede A, Jr., Pinotsis N, Ghisleni A, Salmazo A, Konarev PV, Kostan J, Sjoblom B, Schreiner C, Polyansky AA, Gkougkoulia EA, et al. The structure and regulation of human muscle alpha-actinin. Cell. 2014;159(6):1447-60.
64. Foley KS, and Young PW. The non-muscle functions of actinins: an update. The Biochemical journal. 2014;459(1):1-13.
65. Quick Q, and Skalli O. Alpha-actinin 1 and alpha-actinin 4: contrasting roles in the survival, motility, and RhoA signaling of astrocytoma cells. Experimental cell research. 2010;316(7):1137-47.
66. Shao H, Wu C, and Wells A. Phosphorylation of alpha-actinin 4 upon epidermal growth factor exposure regulates its interaction with actin. The Journal of biological chemistry. 2010;285(4):2591-600.
67. Yamaguchi H, Ito Y, Miura N, Nagamura Y, Nakabo A, Fukami K, Honda K, and Sakai R. Actinin-1 and actinin-4 play essential but distinct roles in invadopodia formation by carcinoma cells. European journal of cell biology. 2017;96(7):685-94.
68. Hsu CP, Moghadaszadeh B, Hartwig JH, and Beggs AH. Sarcomeric and nonmuscle alpha-actinin isoforms exhibit differential dynamics at skeletal muscle Z-lines. Cytoskeleton. 2018;75(5):213-28.
69. Wallgren-Pettersson C, Sewry CA, Nowak KJ, and Laing NG. Nemaline myopathies. Seminars in pediatric neurology. 2011;18(4):230-8.
70. Yamaguchi M, Robson RM, Stromer MH, Dahl DS, and Oda T. Nemaline myopathy rod bodies. Structure and composition. Journal of the neurological sciences. 1982;56(1):35-56.
71. Domazetovska A, Ilkovski B, Kumar V, Valova VA, Vandebrouck A, Hutchinson DO, Robinson PJ, Cooper ST, Sparrow JC, Peckham M, et al. Intranuclear rod myopathy: molecular pathogenesis and mechanisms of weakness. Annals of neurology. 2007;62(6):597-608.
72. Valle G, Faulkner G, De Antoni A, Pacchioni B, Pallavicini A, Pandolfo D, Tiso N, Toppo S, Trevisan S, and Lanfranchi G. Telethonin, a novel sarcomeric protein of heart and skeletal muscle. FEBS letters. 1997;415(2):163-8.
73. Takada F, Vander Woude DL, Tong HQ, Thompson TG, Watkins SC, Kunkel LM, and Beggs AH. Myozenin: an alpha-actinin- and gamma-filamin-binding protein of skeletal muscle Z lines. Proceedings of the National Academy of Sciences of the United States of America. 2001;98(4):1595-600.
74. Bang ML, Mudry RE, McElhinny AS, Trombitas K, Geach AJ, Yamasaki R, Sorimachi H, Granzier H, Gregorio CC, and Labeit S. Myopalladin, a novel 145-kilodalton sarcomeric protein with multiple roles in Z-disc and I-band protein assemblies. The Journal of cell biology. 2001;153(2):413-27.
75. Schroder R, Reimann J, Salmikangas P, Clemen CS, Hayashi YK, Nonaka I, Arahata K, and Carpen O. Beyond LGMD1A: myotilin is a component of central core lesions and nemaline rods. Neuromuscular disorders : NMD. 2003;13(6):451-5.
76. Wallgren-Pettersson C, Jasani B, Newman GR, Morris GE, Jones S, Singhrao S, Clarke A, Virtanen I, Holmberg C, and Rapola J. Alpha-actinin in nemaline bodies in congenital nemaline myopathy: immunological confirmation by light and electron microscopy. Neuromuscular disorders : NMD. 1995;5(2):93-104.

77. Jockusch BM, Veldman H, Griffiths GW, van Oost BA, and Jennekens FG. Immunofluorescence microscopy of a myopathy. alpha-Actinin is a major constituent of nemaline rods. Experimental cell research. 1980;127(2):409-20.
78. Stuhlfauth I, Jennekens FG, Willemse J, and Jockusch BM. Congenital nemaline myopathy. II. Quantitative changes in alpha-actinin and myosin in skeletal muscle. Muscle & nerve. 1983;6(1):69-74.
79. Jockusch BM, Burger MM, DaPrada M, Richards JG, Chaponnier C, and Gabbiani G. alpha-Actinin attached to membranes of secretory vesicles. Nature. 1977;270(5638):628-9.
80. Hein S, Block T, Zimmermann R, Kostin S, Scheffold T, Kubin T, Klovekorn WP, and Schaper J. Deposition of nonsarcomeric alpha-actinin in cardiomyocytes from patients with dilated cardiomyopathy or chronic pressure overload. Experimental and clinical cardiology. 2009;14(3):e68-75.
81. Amsili S, Zer H, Hinderlich S, Krause S, Becker-Cohen M, MacArthur DG, North KN, and Mitrani-Rosenbaum S. UDP-N-acetylglucosamine 2-epimerase/N-acetylmannosamine kinase (GNE) binds to alpha-actinin 1: novel pathways in skeletal muscle? PloS one. 2008;3(6):e2477.
82. Rao P, and Monks DA. A tetracycline-inducible and skeletal muscle-specific Cre recombinase transgenic mouse. Developmental neurobiology. 2009;69(6):401-6.
83. Zhang J, Xin L, Shan B, Chen W, Xie M, Yuen D, Zhang W, Zhang Z, Lajoie GA, and Ma B. PEAKS DB: de novo sequencing assisted database search for sensitive and accurate peptide identification. Molecular & cellular proteomics : MCP. 2012;11(4):M111 010587.
84. Blondelle J, and Lange S. Cullin-3 skm-KO proteome dataset, Mendeley Data, v1. 2019. doi:10.17632/vwg2bbzw3d.1
85. Tripathi S, Pohl MO, Zhou Y, Rodriguez-Frandsen A, Wang G, Stein DA, Moulton HM, DeJesus P, Che J, Mulder LC, et al. Meta- and Orthogonal Integration of Influenza "OMICs" Data Defines a Role for UBR4 in Virus Budding. Cell host & microbe. 2015;18(6):723-35.
86. Stark C, Breitkreutz BJ, Reguly T, Boucher L, Breitkreutz A, and Tyers M. BioGRID: a general repository for interaction datasets. Nucleic acids research. 2006;34(Database issue):D535-9.
87. Schoenauer R, Lange S, Hirschy A, Ehler E, Perriard JC, and Agarkova I. Myomesin 3, a novel structural component of the M-band in striated muscle. Journal of molecular biology. 2008;376(2):338-51.

FIGURES AND FIGURE LEGENDS

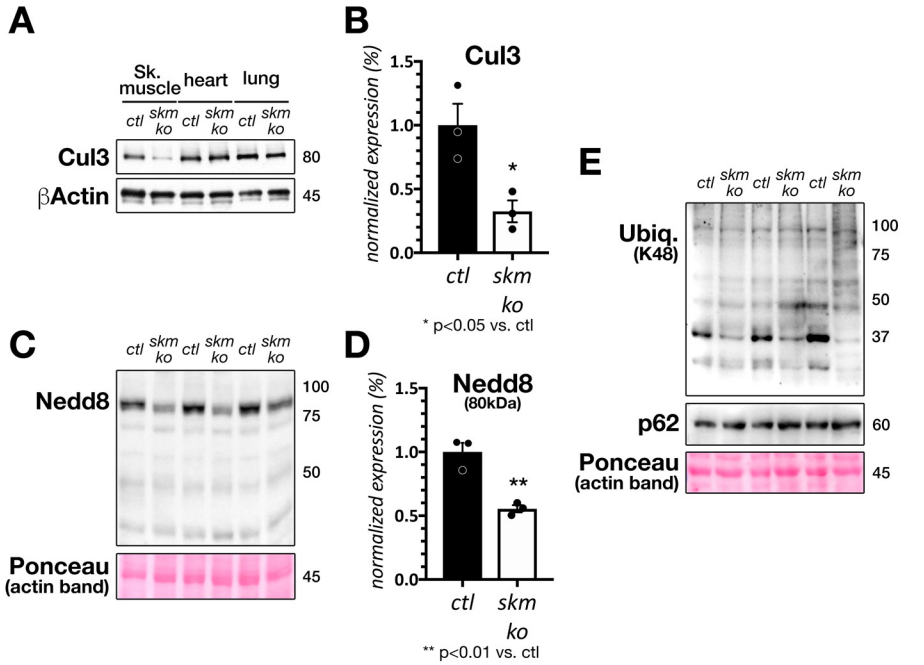

Figure 1. Deletion of *Cullin-3* in skeletal muscles affects the ubiquitin-proteasome system.

(**A**) Immunoblot analysis showing loss of Cullin-3 protein only in skeletal muscle (sk. muscle) of E18.5 *skm-KO*. (**B**) Quantification of Cullin-3 protein levels in E18.5 skeletal muscles (n=3 for each genotype). * *P<0.05* by two-tailed t-test. (**C**) Immunoblot analysis showing a decrease in NEDD8 associated proteins in E18.5 skeletal muscles of *skm-KO*. (**D**) Quantification of 80KDa NEDD8 associated proteins level in E18.5 skeletal muscles (n=3 for each genotype). ** *P<0.01* by two-tailed t-test (**E**) Immunoblot analysis showing a decrease in low molecular weights of K48-ubiquitin associated proteins and no change in p62 expression levels in skeletal muscles of E18.5 *skm-KO*.

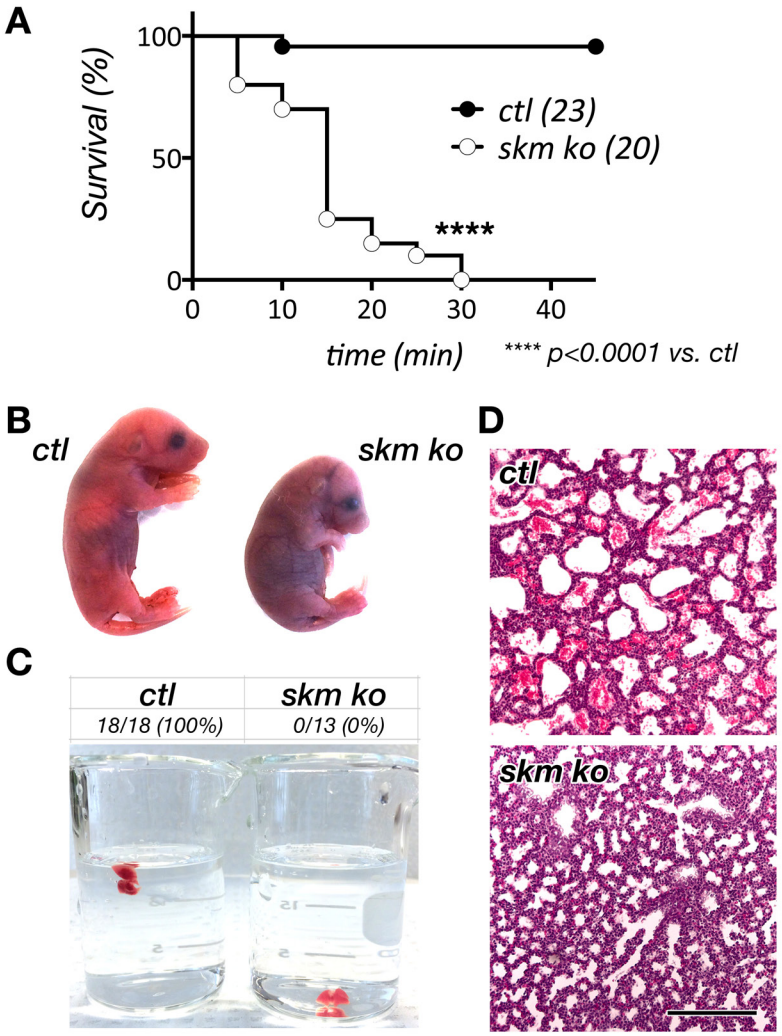

Figure 2. Loss of Cullin-3 during skeletal muscle development leads to postnatal death and respiratory defects.

(**A**) Survival curve of E18.5 embryos following C-section (n=23 for *ctl* and n=20 for *skm-KO*). **** *P<0.0001* by log rank (Mantel-cox) and Gehan-Breslow-Wilcoxon tests. (**B**) Representative pictures of E18.5 embryos showing cyanosis and kyphosis of *skm-KO*. (**C**) Floating assay using lungs extracted from E18.5 *skm-KO* embryos and controls 5 minutes after the C-section and placed at the surface of water (n=18 for *ctl* and n=13 for *skm-*

KO). (**D**) Cross-section of E18.5 lungs 5 minutes after C-section and stained with Hematoxylin-Eosin revealing collapsed alveoli in *skm-KO* embryos.

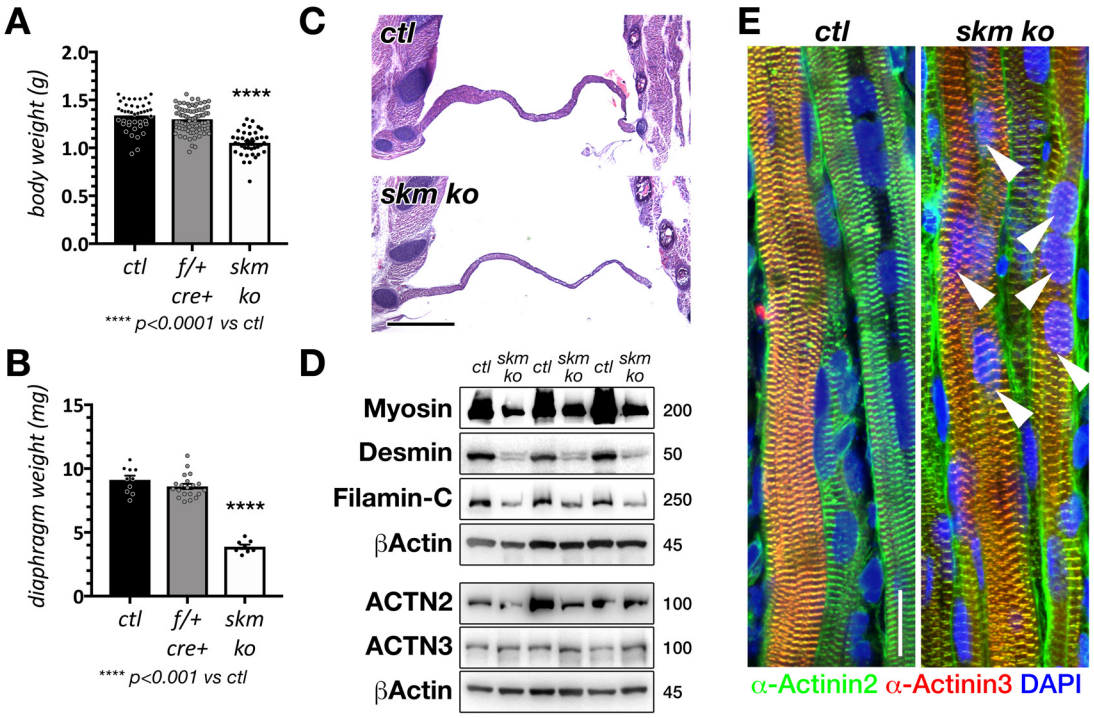

Figure 3. Absence of Cullin-3 leads to severe skeletal muscle myopathy.

(**A**) Body weight analysis of E18.5 embryos (n=43 for *ctl*, n=79 for heterozygous (*f/+;cre+*) and n=41 for *skm-KO*). ****$P<0.001$* by Anova and Bonferroni's multiple comparisons test. (**B**) Diaphragm weight analysis revealing a strong muscle atrophy of E18.5 *skm-KO* embryos. (n=10 for *ctl*, n=19 for heterozygous (*f/+;cre+*) and n=8 for *skm-KO*). ***$P<0.0001$* by Anova and Bonferroni's multiple comparisons test. (**C**) Cross-section of E18.5 diaphragms stained with Hematoxylin-Eosin showing a thinner muscle in *skm-KO*. Scale bar = 1mm. (**D**) Immunoblot analysis unraveling a decrease in expression of muscle maturation markers in *skm-KO* diaphragms (n=3 for each genotype). (**E**) Immunofluorescence staining of diaphragm myofibers with muscle

ACTN2 and ACTN3 antibodies as well as DAPI. Arrowheads indicate centralized nuclei. Scale bar = 20μm.

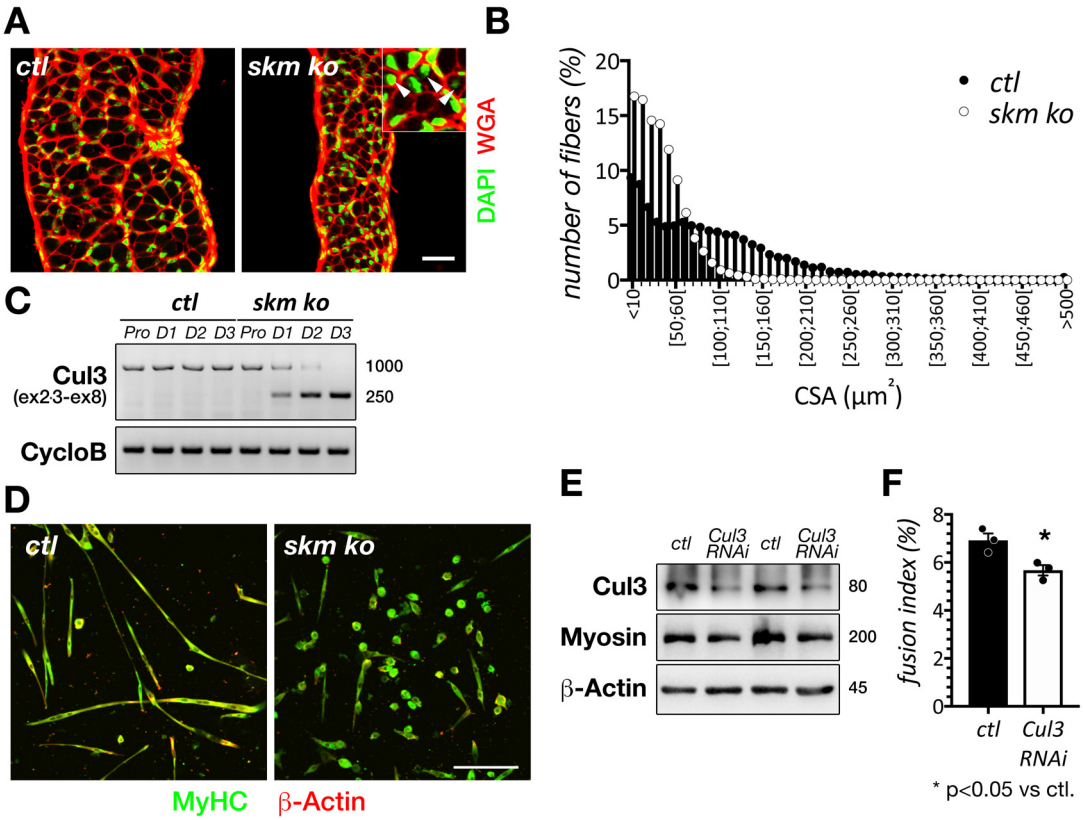

Figure 4. Loss of Cullin-3 leads to muscle fiber hypotrophy *in vivo* and myoblast fusion defect *in vitro*. (**A**) Immunofluorescence staining of E18.5 diaphragms with WGA and DAPI revealing hypotrophy of the myofibers of *skm-KO*. Arrowheads indicate centralized nuclei. Scale bar = 100µm. (**B**) Distribution of fibers constituting diaphragms of E18.5 *ctl* and *skm-KO* depending on their cross-sectional area (CSA in µm^2) (n=3 embryos for each genotype and >11554 fibers per genotype). (**C**) RT-PCR analysis of *Cullin-3* and *Cyclophilin B* (CycloB) in satellite cells isolated from E18.5 *ctl* and *skm-KO* diaphragms over 3 days of differentiation in culture. Pro: Proliferation; D1-3: Differentiation day 1 to 3. (**D**) Immunofluorescence of satellite cells fixed after three days of differentiation and stained with MyHC and β-Actin antibodies. Scale bar = 100µm. (**E**) Immunoblots of

Cullin-3, MyHC and β-Actin on C2C12 myotubes transfected with a *siRNA* against *Cullin-3* or a *scrambled siRNA*, showing efficient knockdown. (**F**) Fusion index (number of nuclei per myotube) of C2C12 cells transfected with a *Cullin-3* or a *scrambled siRNA* and differentiated for 5 days (n=3 per condition and >144 myotubes analyzed per experiment). ****$P<0.05$ by two-tailed t-test.

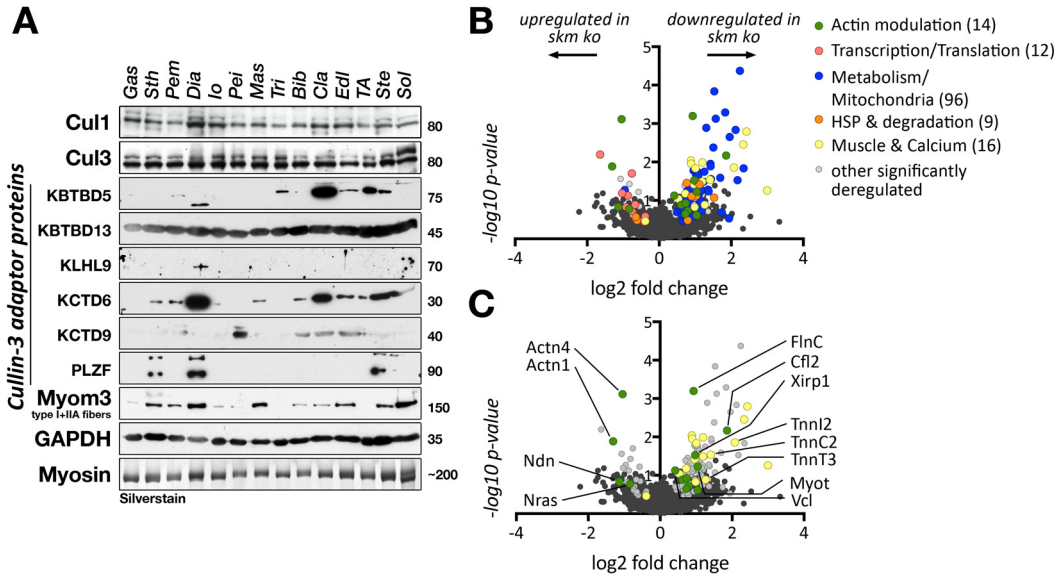

Figure 5. Diaphragm muscle is a hot spot for Cullin-3 substrate adaptors and depletion of Cullin-3 leads to deregulation of protein levels.

(A) Immunoblot analysis showing the pattern of expression of Cullin-1, Cullin-3 and select Cullin-3 substrate adaptors in various mouse skeletal muscles. Myomesin-3 (87) was used as fiber-type marker. Gas: Gastrocnemius; Sth: sternohyoideus; Pem: pectoralis major; Dia: diaphragm; IO: internal oblique; Pei: pectoralis minor; Mas: massester; Tri: triceps, Bib: biceps brachii; Cla: clavotrapezius; EDL: extensor digitorum longus; TA: tibialis anterior; Ste: sternomastoideus; Sol: soleus. (B) Volcano plot of all identified deregulated proteins in E18.5 diaphragms of *skm-KO* following iTRAQ mass spectrometry (3 diaphragms have been pooled per sample and 3 samples for each genotype have been analyzed). (C) Volcano plot highlighting deregulated proteins involved in actin cytoskeleton-modulation as well as proteins related to muscle and

calcium handling (3 diaphragms have been pooled per sample and 3 samples for each genotype have been analyzed).

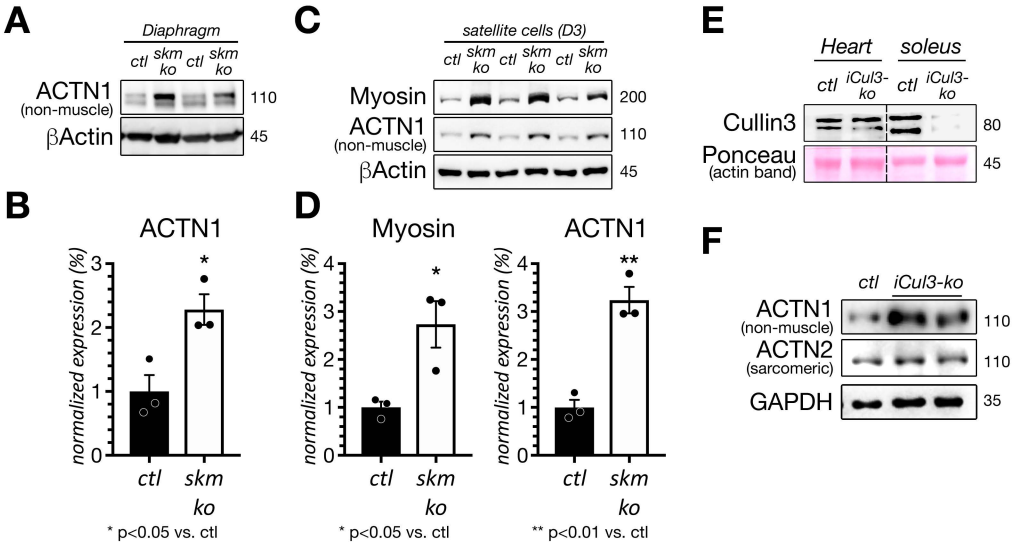

Figure 6. Loss of Cullin-3 induces accumulation of ACTN1.

(**A**) Immunoblot analysis showing accumulation of ACTN1 in diaphragms of *skm-KO* embryos. (**B**) Quantification of ACTN1 protein levels in E18.5 diaphragms of *ctl* and *skm-KO* (n=3 embryos for each genotype). **P<0.05* by two-tailed t-test. (**C**) Immunoblots showing accumulation of ACTN1 and deregulation of sarcomeric myosin in satellite cells of *skm-KO* embryos after 3 days of differentiation. (**D**) Quantification of ACTN1 protein and myosin levels in satellite cells of *ctl* and *skm-KO* after 3 days of differentiation. (n=3 technical replicates for each genotype). **P<0.05*, ***P<0.01* by two-tailed t-test. (**E**) Immunoblot analysis showing the specific loss of Cullin-3 in skeletal muscles of *iCul3-KO* (Doxycycline inducible *Cullin-3* knockout) mice. Dotted line indicates that samples for hearts and soleus have been run on the same gel, but not in adjacent lanes. (**F**) Immunoblot analysis showing accumulation of ACTN1, but not sarcomeric ACTN2, in skeletal muscles of *iCul3-KO* mice treated with Doxycycline.

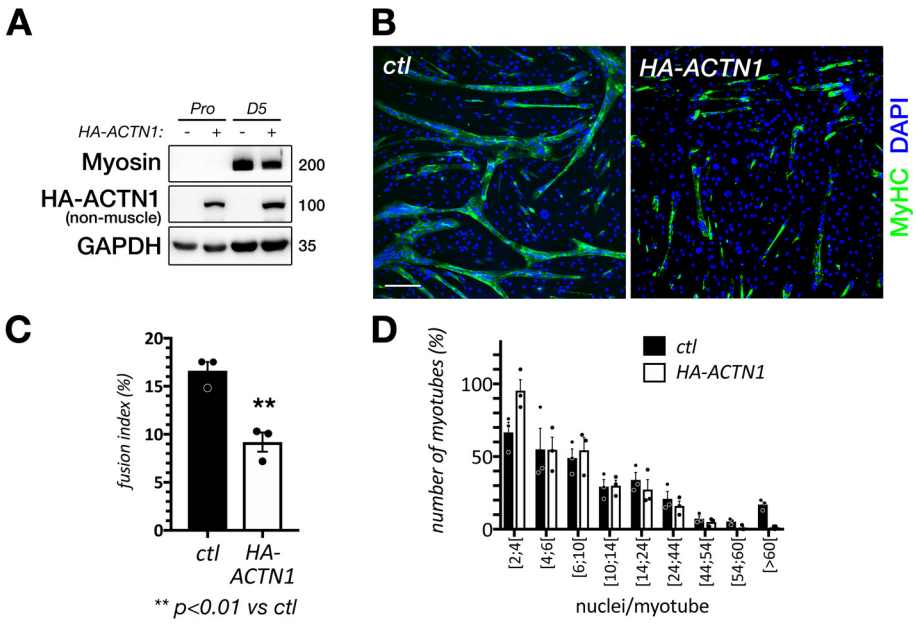

Figure 7. Overexpression of ACTN1 in muscle cells leads to differentiation defects.

(**A**) Immunoblot analysis showing overexpression of ACTN1 in C2C12 cells overexpressing HA-ACTN1 construct. Pro: proliferation; D5: differentiation day 5. (**B**) Immunofluorescence staining of HA (ctl) and HA-ACTN1 overexpressing myotubes with sarcomeric myosin antibody and DAPI after 5 days of differentiation. Scale bar = 200µm. (**C**) Fusion index of cells expressing HA (ctl) and HA-ACTN1 constructs five days after differentiation showing a decrease in the number of nuclei per myotube (n=3 for each condition). ***P<0.01* by two-tailed t-test. (**D**) Distribution of myotubes depending on the number of nuclei (n=3 for each condition).

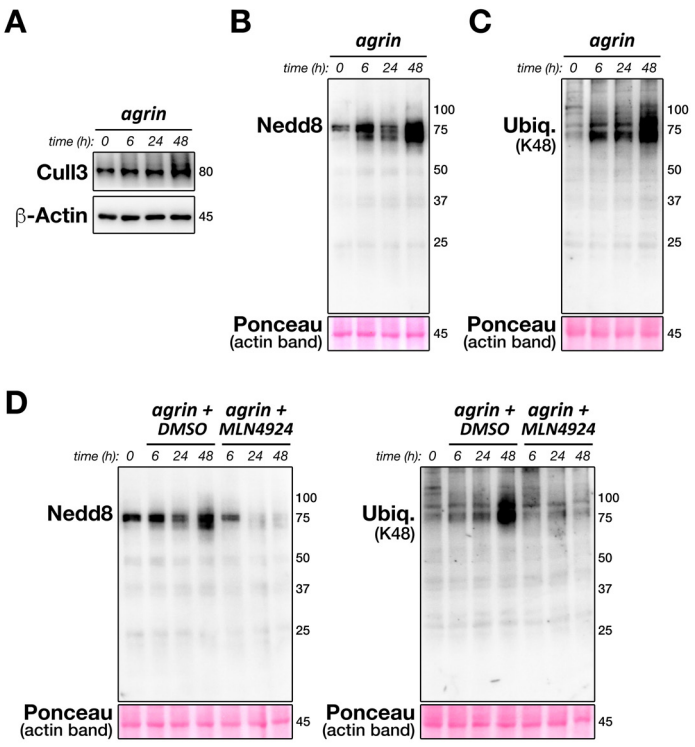

Figure 8. Cullin-3 protein levels and Cullin-RING ligase activity are increased over AchR clustering *in vitro.*

(**A**) Immunoblot analysis showing increased expression of Cullin-3 protein levels in C2C12 cells stimulated with neural agrin (0.5µg/mL) for 48 hours in order to trigger acetylcholine receptor (AchR) clustering. (**B**) Immunoblot analysis showing increased neddylated proteins in C2C12 cells stimulated with agrin for 48 hours. (**C**) Immunoblot analysis showing increased levels of poly-ubiquitylated proteins (K48-linked) in C2C12 myotubes stimulated with agrin for 48 hours. (**D**) Immunoblot analyses showing a decrease in both, Nedd8–linked and poly-ubiquitylated proteins in C2C12 myotubes stimulated with agrin and treated with MLN4924 compared to DMSO.

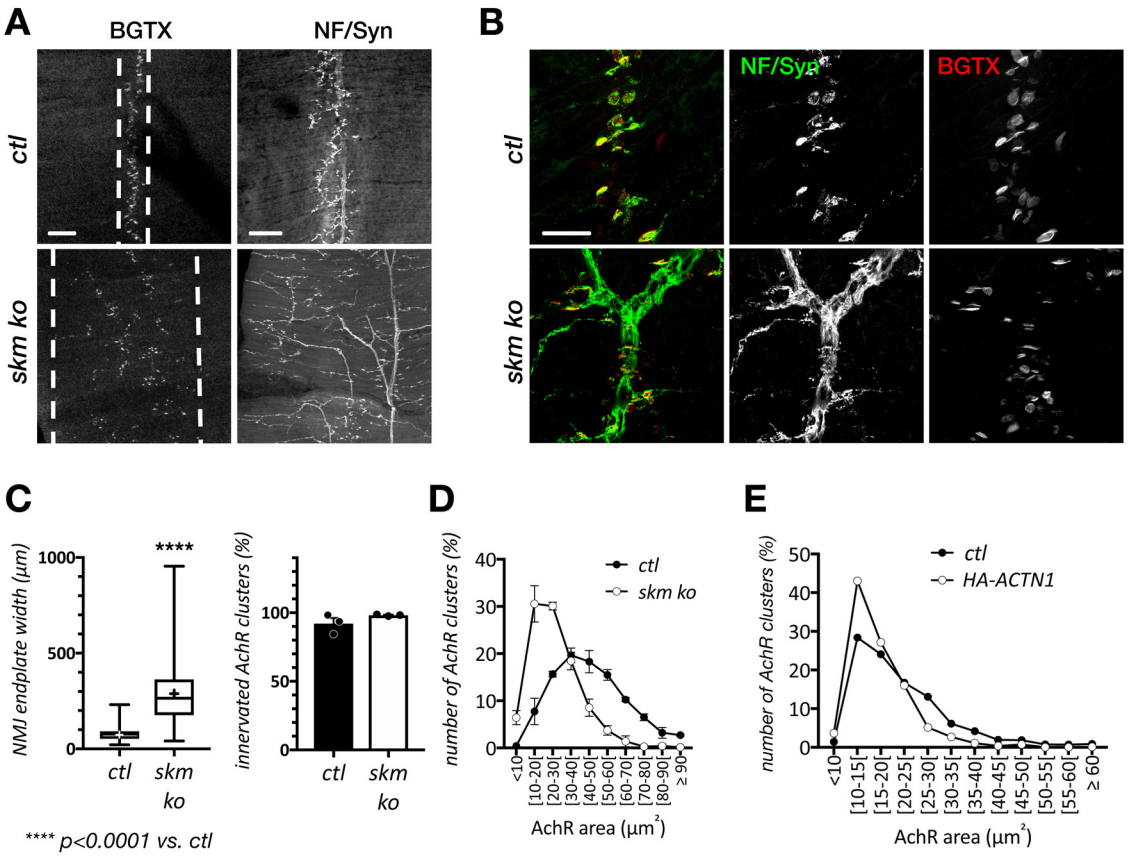

Figure 9. Cullin-3 is required for normal neuromuscular junction (NMJ) formation and acetylcholine receptor (AchR) clustering. (**A, B**) Immunofluorescence staining of the pre- and postsynaptic elements of E18.5 NMJs in *ctl* and *skm-KO* diaphragms with antibodies against Neurofilament and Synaptophysin (NF/Syn) and fluorescent Bungarotoxin (BGTX) showing (**A**) increased area of the motor endplate, dispersion of AchR clusters across the diaphragm and hyper-arborization of the motoneuron in *skm-KO*, but (**B**) normal innervation of the NMJ. (**A**) Scale bar = 100µm. (**B**) Scale bar = 20µm. (**C**) Quantification of NMJ endplate widths (left panel; Box and whiskers plot showing min to max values; average is shown as +) and innervated AchRs (right panel) in the diaphragms of *ctl* and *skm-KO* (n=3 embryos for each genotype, >895 AchRs per genotype). ****$P<0.0001$, by two-tailed t-test (left panel); P=0.211 by two-tailed t-test

(right panel). (**D**) Distribution of AchR clusters of *ctl* and *skm-KO* diaphragms depending on their area (n=3 embryos for each genotype). (**E**) Distribution of AchR cluster areas in 5 day differentiated myotubes expressing HA (*ctl*) or HA-ACTN1 (n=3 per condition and >817 AchR clusters were analyzed per condition).

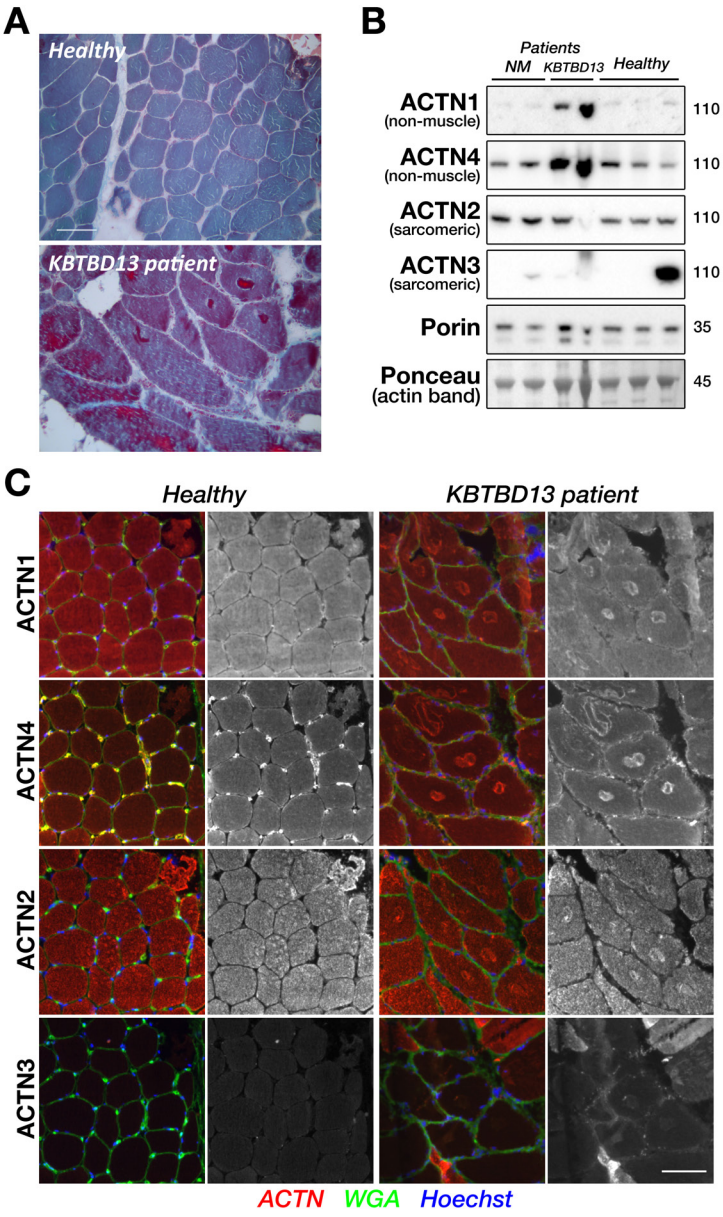

Figure 10. Specific accumulation of non-muscle alpha-Actinins in muscle tissues of patients with *Cul3*-related nemaline myopathies. (**A**) Gomori Trichrome stain of skeletal muscle cross-sections from a healthy individual and a patient with a mutation in *KBTBD13*. (**B**) Immunoblot analyses of alpha-Actinin isoforms expression levels in skeletal muscle biopsies from nemaline patients (NM patients; lane 1: *TPM2* mutation; lane 2: *NEB* mutation), patients with mutations in KBTBD13 (lanes 3 and 4), and healthy

individuals (lanes 5 and 6). Specific accumulation of non-muscle alpha-Actinins (ACTN1 and ACTN4) was observed in samples of patients with mutations in *KBTBD13*. Muscle alpha-Actinins (ACTN2 and 3) did not show abnormal accumulation. Porin and Ponceau stain are shown as loading controls. (**C**) Immunofluorescence staining of cross-sections from muscle biopsies of a healthy individual and a patient with a mutation in *KBTBD13*, revealing a positive staining of nemaline bodies with non-muscle Alpha-actinins (ACTN1 and 4). Scale bars = 100µm (for A and C).

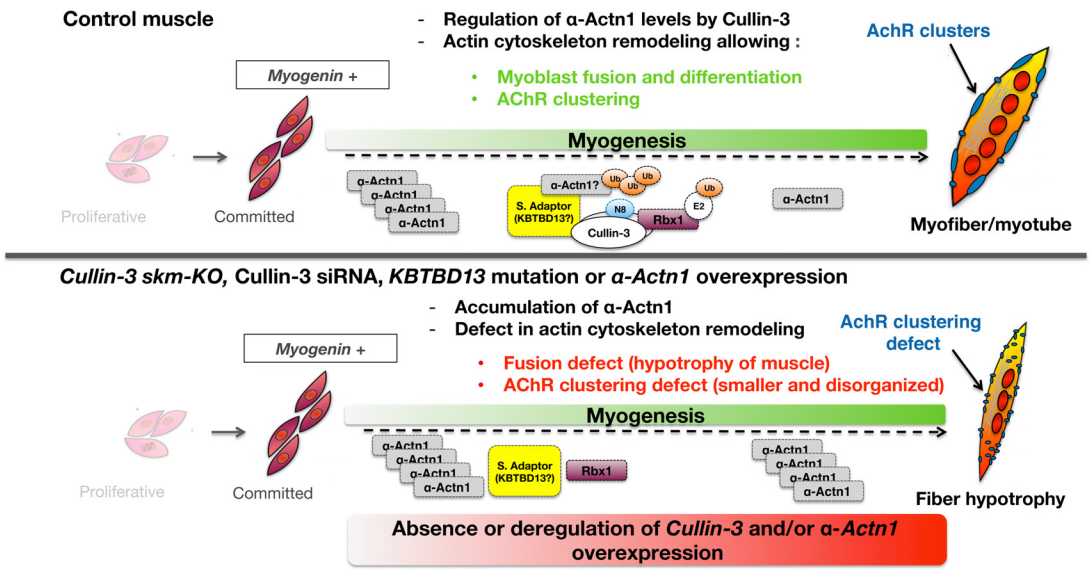

Figure 11. Model for the role of Cullin-3 during muscle fiber development.

S. Adaptor: substrate adaptor, Rbx1: RING-box protein 1, AchR: Acetylcholine Receptor, Ub: Ubiquitin, N8: Nedd8